TU
WIEN

TECHNISCHE UNIVERSITÄT WIEN

DIPLOMARBEIT

PHITS Modelling of an Experimental Setup for Proton Radiotherapy using an Anthropomorphic Phantom

Ausgeführt am

Atominstitut

der Technischen Universität Wien

unter der Anleitung von

Herr Univ.Prof. civ.ing. tekn.lic. tekn.dr. Lembit Sihver

und

Univ.Ass.Dr. Monika Puchalska

durch

Simon Lechner

Ulmenweg 8,

2493 Lichtenwörth

21. März 2017

_____   _____

Unterschrift, Betreuer   **Unterschrift, Student**

Abstract

A RANDO® human phantom was applied for proton therapy calculations. CT-scans of the phantom were used to create a treatment plan with RayStation 5 for an imaginary brain tumor. The prescribed median dose was set to 60 Gy. The beam, used in the treatment plan, adopts the conditions met at the MedAustron accelerator in terms of beam parameters. Then this plan was transferred into an input file for the Monte-Carlo transport code PHITS, in which the NUNDO (numerical voxel model of the RANDO®) phantom was used. The NUNDO consists of 30 organs and 1596 thermoluminescence detectors, which are placed in it in a regular grid. The dose deposition in phantom and the fluence of protons, neutrons and photons were simulated. To validate the transfer procedure from RayStation to PHITS, first a treatment plan for a simple watertank was created and the results were compared.

It was shown that PHITS is able to reproduce the average dose in the target from RayStation within 1 %, but in detailed dose distributions in and outside the target the differences between PHITS and RayStation are 10 to 20 %. The dose outside the beam line is generated mainly from photons and neutrons. Above 50 cm away from the target, the dose from photons dominates. At the bottom of the phantom torso the lowest dose was about 1 μGy.

The results of this thesis will be further used for future experiments at the proton and ion therapy facility MedAustron in Austria.

Abstrakt

Ein menschliches RANDO® Phantom wurde für Protontherapiesimulationen angewendet. CT-Scans von dem Phantom wurden benutzt um einen Behandlungsplan mit RayStation 5 für einen imaginären Gehirntumor zu erstellen. Die vorge- schriebene Mediandosis betrug 60 Gy. Der Protonenstrahl, der im Behandlungsplan benutzt wurde, adoptiert die Gegebenheiten des Teilchenbeschleunigers vom MedAustron bezüglich der Strahlenparameter. Dieser Plan wurde transferiert in eine Input-Datei für den Monte-Carlo Transportcode PHITS. In PHITS wurde das NUNDO (Numerisches Voxelmodell von RANDO®) Phantom genutzt. NUNDO besteht aus 30 Organen und 1596 Thermolumineszenzdetektoren, die in einem regelmäßigen Gitter angeordnet sind. Die Dosisdeposition im Phantom und der Teilchenfluß der Protonen, Neutronen und Photonen wurden simuliert. Um das Transferprozedere von RayStation nach PHITS zu prüfen, wurde zuerst ein Behandlungsplan für einen einfachen Wassertank erstellt und die Ergebnisse wurden verglichen.

Es konnte gezeigt werden, dass PHITS in der Lage ist, die Mediandosis im Tumor von RayStation auf 1 % genau zu reproduzieren. Detaillierte Dosisverteilungen in und außerhalb des Tumors zeigen aber Unterschiede von 10 bis 20 % zwischen RayStation und PHITS. Die Dosis außerhalb des Teilchenstrahls wurde hauptsächlich von Photonen und Neutronen erzeugt. Für Distanzen, die mehr als 50 cm vom Tumor entfernt sind dominiert die Dosis von Photonen. Am unteren Ende des Torsos betrug die niedrigste Dosis ungefähr 1 μGy.

Die Resultate dieser Arbeit können in zukünftigen Experimenten am MedAustron in Österreich verwendet werden.

Contents

1. Introduction

Proton and heavy-ion beams are an important field of current research. A great interest lies on the protection from space radiation for astronauts and cancer treatment with hadrontherapy.
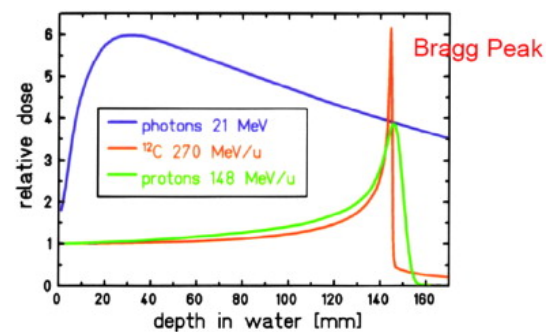
The advantages of using protons or ions for cancer treatment are the highly localized dose deposition compared with other cancer treatment methods. Due to the high dose deposition (Bragg-peak) at the end of the particle range (see *Fig. (1.1)*) one can treat for example deep seated tumors in the vicinity of organs at risk and spare these organs.

Since the 1950's protons and since the 1970's heavy-ions are used for cancer treatment. Because of their higher mass, heavy-ions have a lower angular scattering and a higher dose deposition at the end of their range compared with protons as shown in *Fig. (1.1)*, but they have also a tail after the Bragg-peak caused by projectile fragments. This tail is not present in proton beams. Proton beams are used in the majority of the treatments [1] due to a better understanding and an easier handling of them.

Nevertheless proton therapy has started in the 1950's, the study of the influence of protons (or neutrons) on healthy tissue, and the connected risk of secondary cancers, is still ongoing. An improvement have been made by introducing the method of pencil beam scanning, which enables a more precise dose deposition and reduces the dose outside of the irradiated tumor volume.

Figure 1.1.: Comparison between the depth dose distribution of photons, carbon ions and protons taken from [2].

A new facility for hadron therapy and research has been recently built in Austria, the MedAustron [3]. Its accelerator handles proton and carbon ions and uses pencil beam scanning for treatments. One treatment room is reserved for research, including the dose deposition in phantoms or beams impinging on different targets.

Due to the high costs and effort of such experiments, it is convenient to apply

transport codes or analytic formulas. Most of the transport codes are based on Monte-Carlo technique, e.g. PHITS [4], Geant4 [5] and FLUKA [6]. The Monte-Carlo codes are using different physical models and nuclear libraries, based on experimental data. The models have to be benchmarked against experimental data to be able to accurate reproduce the physical processes. Unfortunately, the Monte-Carlo based codes are time-consuming and require fast computers.

In this work a treatment plan for a RANDO® phantom with an imaginary brain tumor is created with the treatment planning software (TPS) from RayStation. The properties of the proton beam are adopted from the conditions met at the MedAustron. This plan is then transferred to PHITS for a detailed study of the dose distribution in the phantom. To exclude the complex geometry influence on the RayStation to PHITS transfer procedure, first a treatment plan for a simple water tank was created and the results were compared to the data from the TPS. The results of this study can be used for planned experiments with human phantoms at the MedAustron.

For the simulation in PHITS, the NUNDO (numerical RANDO®) phantom was used. This numerical phantom was originally created for simulations of the nearly isotropic radiation exposure of astronauts. A C++ code is developed to calculate the average organ shielding of the NUNDO phantom and the results are compared with [7].

The second chapter treats the theory of proton therapy and gives a short overview of the MedAustron and the software used in this study. In the third chapter the calculation of the organ shielding is described. In the chapter four, the methods used in the thesis are described. Afterwards the results are presented and at last comes the conclusion.

2. Theory

2.1. Proton Therapy

In 1946 Wilson [8] suggested to use protons in radiotherapy. At this time, new particle accelerators, which were able to deliver protons with energies over 200 MeV, were under construction. Protons with 200 MeV have a range of about 27 cm in human tissue [8], thus it is possible to reach any part of the body with such beams. Due to their finite range and the Bragg-peak, protons beams are suitable to treat deep seated tumors, while sparing healthy tissue.

In the following section, common quantities used in radiotherapy (*Section 2.1.1*) are introduced. Then follows a description of the behavior of protons when they interact with matter (*Section 2.1.2*) , including the Bragg-curve. In *Section 2.1.3* the advantages of proton beams and their use in radiotherapy will be described.

2.1.1. Important Quantities

The stopping power [9]

$$S = -\frac{dE}{dx} \qquad \left[\frac{MeV}{cm}\right] \tag{2.1}$$

defines the loss of kinetic energy of charged particles per path length and the mass stopping power

$$\frac{S}{\rho} = -\frac{1}{\rho}\frac{dE}{dx} \qquad \left[\frac{MeV}{g/cm^2}\right] \tag{2.2}$$

considers also the density of the medium.

The number of particles dN crossing a infinitesimal area dA normal to the beam line is called particle fluence

$$\phi = \frac{dN}{dA} \qquad \left[\frac{particles}{cm^2}\right]. \tag{2.3}$$

One important quantity in radiotherapy is the absorbed dose

$$D = \frac{dE}{dm} \qquad \left[Gy = \frac{J}{kg} \right],$$ (2.4)

which is the energy absorbed per unit mass of a material and it has the unit of Gray (Gy). Typical doses during a cancer treatment are between 60 and 70 Gy in the tumor volume. A dose of 4 Gy, received in a short time, in the whole body is lethal [9]. The absorbed dose can also be expressed by the mass stopping power and the fluence

$$D = \phi \frac{S}{\rho}.$$ (2.5)

2.1.2. Interaction of Protons with Matter

Protons interact with matter in three different ways [9]. They lose kinetic energy and slow down by collisions with atomic electrons, they are deflected by collisions with atomic nuclei (multiple Coulomb scattering) and they undergo nuclear reactions with atomic nuclei.

The interaction of protons with atomic electrons depends on the velocity of the protons and is mediated by the Coulomb force. A fast proton has only a short time to interact with an electron and thus, it loses only little energy. By traveling further through matter the proton slows down and loses more energy, because it perceives the electrons longer. At the end of the range, it loses most of its energy.

Bethe and Bloch derived the theoretical loss of energy for charged particles in matter (stopping power) in the Bethe-Bloch formula. A simplified formula [9] for protons in the radiotherapy energy range (3 - 300 MeV) is

$$\frac{S}{\rho} = -\frac{1}{\rho} \frac{dE}{dx} = 0.3072 \frac{Z}{A} \frac{1}{\beta^2} \left(\ln \frac{W_m}{I} - \beta^2 \right)$$ (2.6)

where Z is the atomic number and A the relative atomic mass of the medium and $\beta = \frac{v}{c}$ is the relative speed of the protons. W_m defines the maximum energy loss in a single collision with a free electron and I is the mean ionization potential of the medium.

Protons with a specific energy stop after a specific distance, due to the energy loss. But due to a large number of individual collisions, there is a statistical error in the proton range. This is called range or energy straggling and can be described with probability distributions, like the Landau [10] and the Vavilov [11] distribution.

Except of energy loss by collisions with electrons, protons are scattered by collisions with atomic nuclei. This deflection of protons is also mediated by the Coulomb force and is called multiple Coulomb scattering (MCS). Because the deflection angle from a single scatter event is very low, the effect of multiple scatter events has a statistical nature. The angular distribution of MCS has approximately a Gaussian shape for small angles, but for a complete description of MCS the rare deflections with high angles must also be considered. This was achieved in Molière's theory [12, 13], which uses no empirical parameters, covers arbitrarily thick scatter materials and can be applied for any charged particle.

The procedure of stopping and scattering is well understood, but nuclear reactions are quite hard to model. The main interest in proton therapy lies in nonelastic nuclear reactions in which secondary particles are produced. Protons, which only mediate stopping or scattering are called primaries. The biggest share of secondaries are Protons followed by neutrons and photons. A small amount of the energy goes also into heavier target fragments like alpha particles. These heavy fragments have a very short range and lead to a high-local dose deposition. Otherwise the dose from neutrons and photons is distributed non-local and contributes mainly to the dose outside of the beam field.

The Bragg-curve (red lines in *Fig. (2.1)*) combines the effects of stopping, scattering and nuclear reaction and shows the absorbed dose per depth in a medium from an impinging proton beam. At the end of the Bragg-curve the Bragg-peak occurs, where most of the proton energy is deposited. The position of the Bragg-peak depends mainly on the energy of the beam. The overall shape of the Bragg-curve is determined by the stopping power (Bethe-Bloch formula) and the effect of energy straggling widens the Bragg-peak, which would be very sharp without it. Nuclear reactions contribute only slightly to the dose through nuclear buildup in the entrance region of the beam.

2.1.3. Proton Beams in Radiotherapy

The main goal in radiotherapy is to destroy the cells of the tumor with high doses, while sparing the healthy tissue around the tumor. *Fig. (2.1)* shows a comparison of protons and photons. A photon beam produces the highest dose near the entrance and then falls of exponentially, while a proton beam is able to deposited the highest dose in the tumor. By adding several proton beams with different energies and intensities,
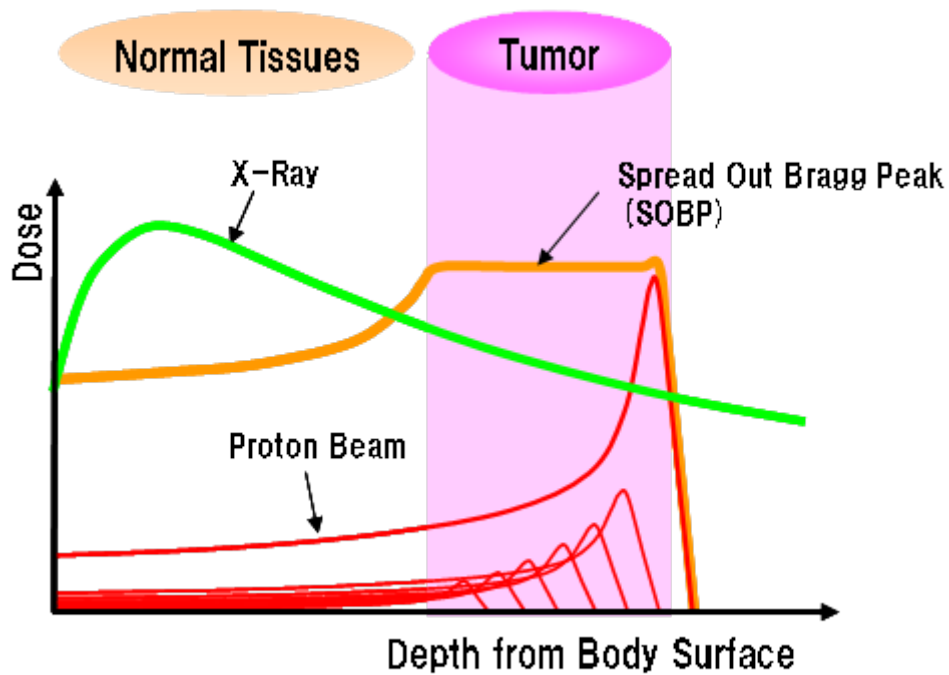
Figure 2.1.: Several Bragg-curves added together form the spread out Bragg-peak (SOPB). This enables a much better dose distribution inside the tumor compared to x-rays. [14]

it is possible to create a spread out Bragg-peak (SOBP).

Any target volume can be covered by SOBPs. Organs at risk, which may be next to the tumor, can be spared from high doses by using the sharp distal and lateral dose fall-off of proton beams. The dose to normal tissue can be further reduced by using two or more beams, which impinge from different directions.

There are two main types of particle accelerators, which are able to provide the beams for proton therapy, cyclotrons and synchrotrons [9]. Cyclotrons generate beams with a fixed energy of about 250 MeV, while synchrotons are able to generate beams with a continuously energy range. Passive scattering systems in which high Z materials spread out the beam and decrease the energy to the desired values, are used for both accelerator types. A disadvantage of passive scattering is that a lot of neutrons are produced in the high Z material, which contribute to the out of field dose [15]. This can be prevented by using the active scanning mode with magnets deflecting particles to required positions.

In the pencil beam scanning (PBS) technique, a two-dimensional magnetic scanning system is placed behind the beam line, which is able to deflect the beam to any spot in the tumor. By scanning the tumor volume spot after spot, a very good dose distribution can be achieved [9].

2.2. MedAustron

The MedAustron [3] is a new hadron therapy and research facility in Austria, which started its clinical treatments in December 2016. Protons and carbon ions can be accelerated in a synchrotron and they are extracted into the treatment rooms with pencil beam scanning. There are three treatment rooms and one research room. The beam parameters for the non-clinical research room are listed in *Tab. (2.1)*.

Table 2.1.: Beam parameters of the MedAustron synchroton for non-clinical research.

particles	protons	carbon ions
particles per pulse	$\leq 10^{10}$	$\leq 4 \times 10^8$
beam energy	60 - 800 MeV	120 - 400 MeV/u
extraction duration	0.1 - 10 s	0.1 - 10 s
magnetic rigidity	1.14 - 4.88 Tm	3.25 - 6.35 Tm

Treatment plans can be created with the treatment planning system RayStation 5.

2.3. RayStation

RayStation 5 [16] is a user friendly treatment planning software for photon, electron, proton and carbon ion therapy. It includes various patient modeling options, detailed plan design and optimization features and other useful functions. This chapter demonstrates how to create a treatment plan with a description of the functions of RayStation. For the detailed description of the algorithms and formulas for dose calculation and optimization, the reader is referred to the RayStation reference manual. This description is by no means complete and treats mainly the steps, which were necessary for this work with a focus on protons.

2.3.1. Producing a Treatment Plan

The first step to create a treatment plan is a medical image set of a patient from computer tomography (CT), positron emission tomography (PET) or magnetic resonance imaging (MRI). CT-images in the DICOM format were used in this work, so the following description of the treatment plan will just consider a image set from a CT-scan.

The DICOM format presents the mass density of a patient in Houndsfield Units (HU). This HU have to be transformed to a mass density in g/cm^3 with a CT-conversion

table. RayStation provides the Generic CT table with a conversion of HU into mass densities of typical tissue and bones.

Patient Modeling

The next step is to create regions of interest (ROI) in the Patient Modeling module. A ROI can be an organ, a planning target volume (PTV) or a simple geometric volume. There are a lot of options for ROIs from basic shapes, like a sphere or box, to complex hand drawn shapes and it is also possible to generate some organs automatically. The most important ROI is the PTV, which will receive the main share of the dose.

Plan Design

If the target is defined, then one needs to add a particle source. This can be achieved in the Plan Design module. A new plan contains the information about the modality (photons, protons, etc.), the treatment technique (for example passive scattering or pencil beam scanning for protons) and the treatment machine, which is unique for each facility and has to be commissioned. Also the prescribed dose and the number of treatment fractions have to be defined. Typically a dose per daily fraction is 1.8-2.0 Gy, so if the total prescribed dose in the tumour should reach 60 Gy, at least 30 fractions are needed [9].

After the treatment machine is chosen, a beam (also multiple beams) can be added. First, the isocenter of the beam has to be specified, which can be any point, but it is advantageous to choose the center of the PTV. Then the gantry and the couch angle can be changed. Due to the advantage of proton beams in minimizing the dose to normal tissue, usually two beams are used for a treatment plan.

Plan Optimization

After the target and the beam are defined, some constraints regarding the dose conformity in the target and the maximum dose to normal tissue, need to be defined. This objectives or constraints can be for instance a minimum dose, a maximum dose or a dose fall-off. The difference between a objective and a constraint is, that a constraint has to be fulfilled, while a objective has a relative weighting factor. So if the first objective has a weight of 10 and the second has a weight of 1, the first one is 10 times more important.

Minimum and maximum doses are needed for the PTV, which should be very close to the prescribed dose. Also organs at risk need a maximum dose constraint to be set. Other objectives or constraints have to be chosen individually for every patient to fulfill the clinical goals.

It is also possible in the Plan Optimization module to change the spot settings. The energy layer spacing, the spot spacing or the target margin can be set to fixed values, if necessary. By default all these parameters are calculated by automatic functions.

2.4. PHITS

The multi-purpose **P**article and **H**eavy-**I**on **T**ransport code **S**ystem (PHITS) [4] is a Monte-Carlo simulation code for the transport of particles and heavy ions in matter. It is able to deal with almost all types of particles over a wide energy range in complex three-dimensional geometries. Several nuclear reaction models and data libraries can be used for simulations (*Fig. (2.2)*).
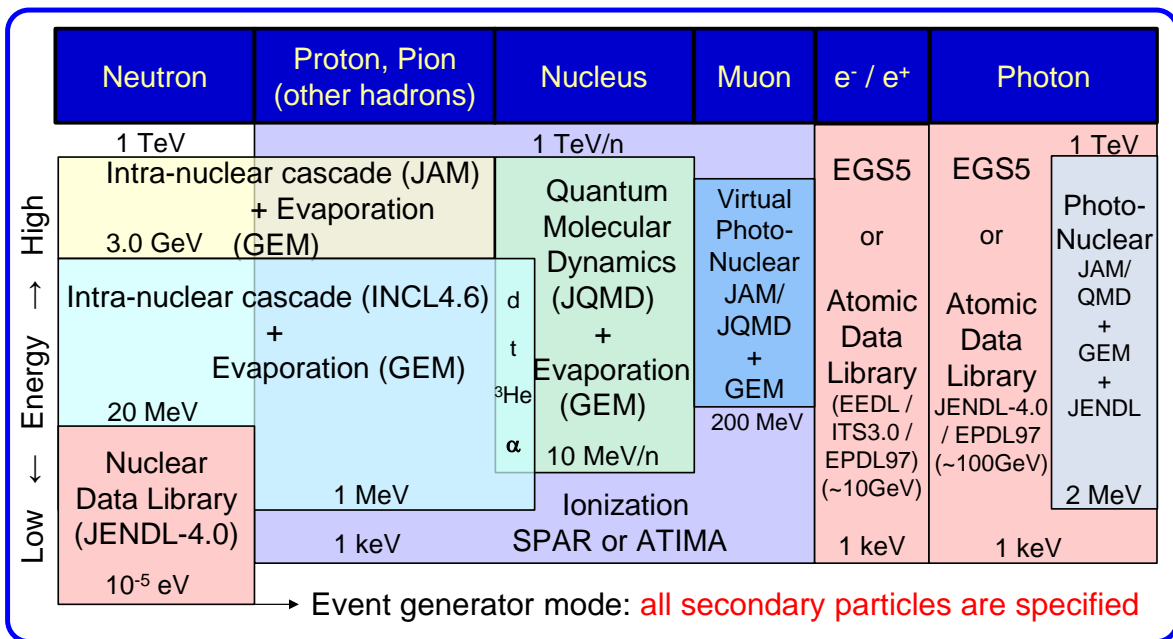

Figure 2.2.: Physical models and data libraries used in PHITS2.85 [17].

Advantages:

- wide field of applications

- no programming skills are required

- good accuracy and statistics

Disadvantages:

- long processing time

- requires skills to create complex geometries

The next section explains what is included in an input file for PHITS and 2.4.2 describes some of the physical models used for the PHITS simulation in this thesis.

2.4.1. Input File

To start a simulation with PHITS, one needs an input file in which all the information regarding the simulation is written. An input file is structured in several sections which will be explained here. There are many more sections in PHITS than described here, but only the following sections are for relevance in this thesis.

Parameters

The first section is called [P a r a m e t e r s] where various parameters and physical models can be defined. The total number of particles is defined by multiplying the number of batches times the number of particles per batch. A batch is one calculation process with the desired number of particles. The higher the total number of particles the better the statistics, but the longer takes the simulation.

To obtain a better accuracy, it is possible to reduce the cut-off energy individually for each particle type. One can chose between a lot of different physical models, like energy straggling, multiple Coulomb scattering (MCS), several nuclear reaction models and many more.

Source

The beam is defined in the [S o u r c e] section. Following parameters of the beam can be chosen:

- shape (cylindrical, rectangular, Gaussian, etc.)

- starting position

- direction of propagation

- lateral spread out

- energy (distribution)

For complex beam setups, like for proton therapy, it is helpful to use so-called dumpfiles (*Section 4.3*) in which the beam parameters are written.

Material

The material composition of the objects used in the simulation are defined in the [M a t e r i a l] section. It is possible to create any composition of elements with their relative weight in a material.

Surface and Cell

The basic shape of a geometry is created in the [S u r f a c e] section, which can be a cylinder, a box or a complex transformation matrix and the content of a surface is further used in the [C e l l] section. A cell consists of a cell ID, the material, the density and a combination of objects included in [S u r f a c e].. The cell ID can be used in the [T a l l y] section to observe a specific region in the simulation.

Tallies

Before the simulation can be started, one has to specify which physical quantity (dose, fluence, LET, etc.) will be measured. This happens in so called tallies. There are tallies for particle fluence ([t-track], [t-cross] and [t-point]), for heat and energy deposition ([t-heat], [t-deposit]), for produced particles ([t-product]), for LET ([t-let]) and some others.

Every tally needs a specified region in which the measurement or the observation of a particle takes place. This can be a cylinder, a box or one or more defined regions from the [C e l l] section. Depending on the tally, it is possible to define energy, angle and/or time steps. The result of each tally is written in a file, after the simulation is finished and PHITS is also able to create a graphical output of the result.

Counter

To observe a certain behavior of a specific particle in a tally, it is helpful to include the [C o u n t e r] section. The counter counts when a particle either enters a specified region, leaves this region, collides in this region, undergoes nuclear fission in this region or is reflected in this region. To measure the dose deposition of neutral particles, like neutrons or photons, the secondary particles have to be followed and their energy deposition counted.

2.4.2. Physics Models

When a projectile with a high energy impinges on a target nucleus, a two-stage spallation process is set off. In the first stage nucleon-nucleon collisions emit fast particles and the second stage handles the de-excitation of thermalized remnants. PHITS uses the Liége intranuclear cascade model (INCL) [18] for nuclear reactions induced by nucleons, pions or light ions, which covers the first stage and combines it with the general evaporation model (GEM) [19], which treats the second stage.

MCS can be implemented in PHITS by Lynch's formula [20] which is based on the Moliére theory or by the ATIMA code [21]. Energy straggling can also be calculated by ATIMA or by using Landau [10] and Vavilov [11] distributions. The ATIMA program was developed at GSI and is able to calculate some physical quantities which characterize the behavior of protons and heavy ions with energies between 1 keV/u and 450 GeV/u in matter. These quantities are energy loss and energy straggling, angular straggling (MCS), range and range straggling, magnetic rigidity and time-of-flight.

The models from [22, 23] are used in PHITS for total reaction cross sections.

3. Calculation of the Organ Shielding

Originally the NUNDO phantom (*Section 3.1*) was developed for simulations of the radiation exposure of astronauts during space missions. A part of this thesis was to write a program, which calculates the organ shielding of the NUNDO phantom and compare it with the results of [7]. Some parts of the program were also used to transfer a treatment plan from RayStation to PHITS (*Section 4.3.2*).

3.1. NUNDO

The NUNDO (Numerical RANDO®) phantom from [24, 25] is a transformation of the RANDO® phantom (*Section 4.2*) into a voxel geometry with a size of $1 \times 1 \times 5\,mm^3$ per voxel and a total size of $35.8 \times 27 \times 84.5\,cm^3$. It consists of 30 organs (*Fig. (3.1)*), including the radiosensitive organs according to the reference man of the International Comission on Radiological Protection (ICRP) [26]. Also 1596 thermoluminescence detectors (TLD) are placed in the phantom in a regular grid. Although the RANDO® phantom is based on a man, the NUNDO phantom contains also female specific organs.

The NUNDO consists only of four different materials. A soft tissue with a mass density of $0.997\,g/cm^3$, bones with $1.3\,g/cm^3$, lungs with $0.352\,g/cm^3$ and TLDs with $2.7\,g/cm^3$. The density of the TLDs was set to $0.997\,g/cm^3$, due to the dose normalization to water.

The information about the voxel phantom is written in a text file containing ID-numbers, which refer to a material (air, organs or TLDs) and each number can be assigned to a specific position in a xyz-coordinate system.
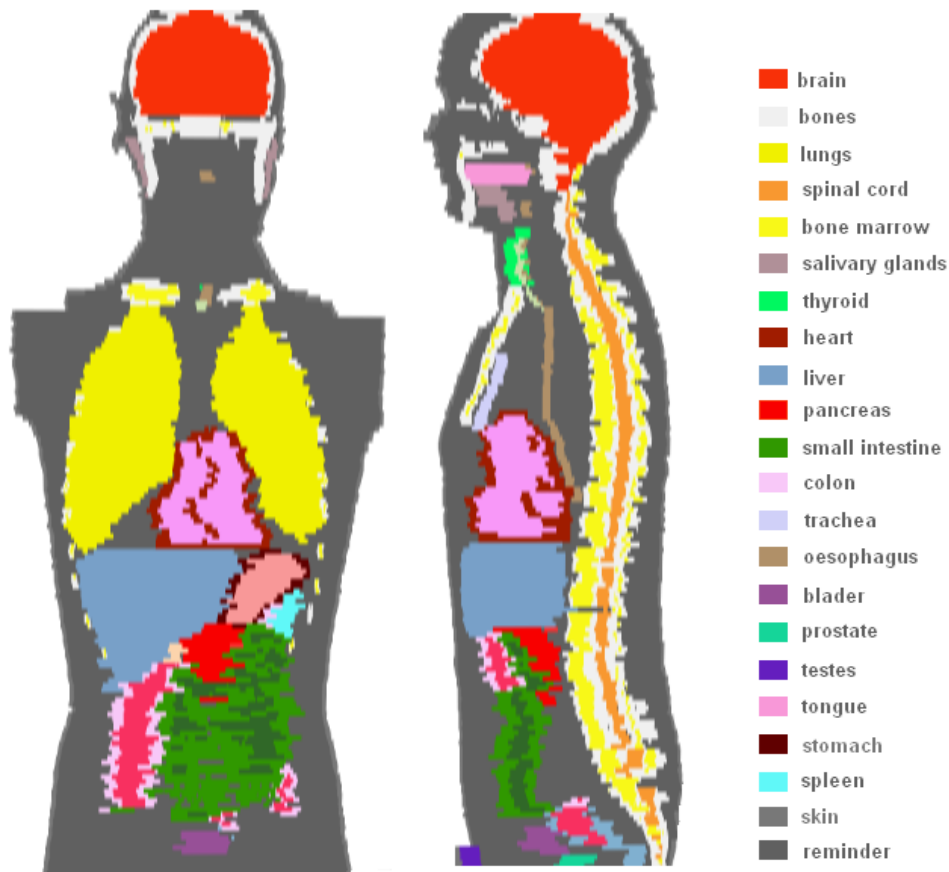
Figure 3.1.: NUNDO phantom (not all organs are visible) [25]

3.2. Program

Based on the numerical values from the voxel phantom file, a C++ program (B.1) was written to calculate the mean organ shielding for 16 organs listed in [7]. By multiplying the average distance from a point inside the phantom to the outside with the density in every voxel cell one gets the average organ shielding for isotropic irradiation in the unit $[cm \times \frac{g}{cm^3} = \frac{g}{cm^2}]$. There are many approaches to calculate the mean organ shielding. The one chosen in this thesis is for sure not the fastest one, but it should be a pretty accurate one. This program has been designed as follows.

First the origin of the coordinate system was placed at the bottom left corner of the phantom (*Fig. (3.2)*). Each of the 16 organs (ID number between 801 and 835) got three vectors (one-dimensional array in C++) assigned (x, y, z) and when a read in ID number matches with an organ, the position of this voxel cell was saved in the three organ vectors.

Each point got also his own density, depending on its ID number:

material	ID number	density
vacuum	99	0
bones	816	1.3
lungs	806	0.352
remainder	-	0.997

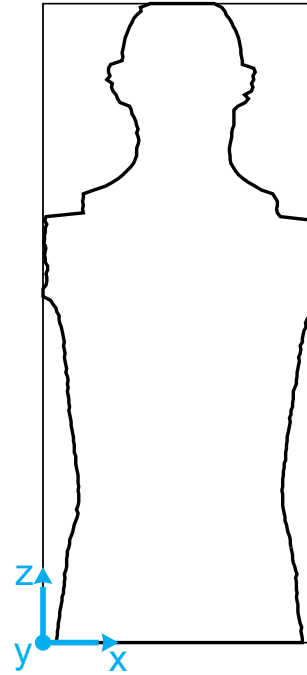The density was saved in a separate vector.

After assigning the coordinates to each element of the voxel phantom, the calculations of the mean shielding has started. From an individual voxel of an organ a random direction in polar and azimuth angles is chosen. Then the mean shielding is calculated in this direction in 1 mm steps until the density reaches zero (air).

One organ shielding distance is calculated but to get the mean organ shielding this step has to be repeated many times to go through a large number of possible directions with the random function. This procedure is repeated 100 times for each voxel. For example, the lung consists of 951,197 voxel cells hence, the mean organ shielding for this organ is calculated from 95,119,700 distances. The source code of this program can be found in B.1.

Figure 3.2.: Front view of the contour of the NUNDO phantom with the starting point in the voxel file and also the coordinate origin in the organ shielding program (blue).

3.3. Results

The results of the calculation are presented in *Tab. (3.1)*, together with the results of Matthiä [7], the relative difference between both approaches and the total number of voxel cells per organ. On the first view one sees that the values from Matthiä are around 20 % lower for most organs than those from this thesis. A very good agreement was achieved for the skin, the breast and the testes.

The difference in the method from Matthiä was, that equally distributed points in the phantom were chosen and the organ type of this points were remembered, while in this thesis every voxel cell of each organ was considered for the calculation. Matthiä also had a smaller step size of 0.5 mm. Despite Matthiä chose a large number

Table 3.1.: Comparison of the mean organ shielding for isotropic irradiation calculated in this thesis (Lechner) and by Matthiä [7].

#	organ	mean organ shielding [g/cm^2]		rel. diff. [%]	number of cells
		Matthiä [7]	Lechner		
1	remainder	11.9	14.24	16.4	4169349
2	skin	9.3	9.08	2.5	478255
3	lungs	11.6	14.42	19.6	951197
4	breast	9.8	9.85	0.5	4873
5	stomach	15.2	18.03	15.7	31606
6	thyroid	11	16.84	34.7	3882
7	oesophagus	13.7	18.98	27.8	6796
8	colon	14.6	17.38	16.0	64120
9	bones	12.7	15.12	16.0	485847
10	brain	9.6	13.02	26.2	247018
11	liver	15.3	17.94	14.7	323392
12	salivary glands	9.6	10.25	6.3	14351
13	red bone marrow	13.5	16.82	19.7	154731
14	bladder	12.6	15.97	21.1	8960
15	testes	7.7	7.59	1.5	5623
16	ovaries	15.5	18.18	14.7	2460

of points, the approach in this thesis is probably the more accurate one since every point is considered.

4. Setup

This is probably the first attempt to convert a treatment plan for protons generated by the RayStation Treatment Planning System (TPS) into an input file of PHITS. Due to that, the first treatment plan was produced for a simple watertank (*Section 4.1*), to check if the converting procedure from the TPS to PHITS works fine and if the deposited dose in the planning target volume (PTV) is comparable. After this successful test a treatment plan for a more complex phantom (*Section 4.2*) was created. It has to be mentioned that the treatment plans were kept simple.

The procedures to create a treatment plan for the watertank and for the human phantom are similar and will be described in *Section 4.1* and *Section 4.2*. The transfer procedure from RayStation to PHITS is shown in *Section 4.3* for both plans. An input file for the PHITS simulation was written, which will be explained in *Section 4.4* with the used models, parameters and tallies. *Section 4.5* describes the manner in which the data were evaluated and how the units from PHITS were converted into Gy.

4.1. Treatment Plan for the Watertank

The watertank (*Fig. (4.1)*) used in the thesis, has a size of $50 \times 50 \times 20\,cm^3$ with a homogeneous density of $1.02\,g/cm^3$. In the center of the tank a PTV with dimensions of $4 \times 4 \times 4\,cm^3$ was placed.

After defining the PTV, a proton beam with pencil beam scanning was created by using the IR3HBL_r10_2 treatment machine, which represents the conditions of the MedAustron synchrotron. This treatment machine has a fixed distance of $64.8\,cm$ from the snout to the isocenter. The prescribed median dose (D50) was set to $60\,Gy$ in 30 fractions, so $2\,Gy$ per fraction. For a good dose conformity, two opposing beams coming from the x-direction (*Fig. (4.1)*) were created.

Following objectives were applied in the Optimization module:

- Minimum Dose to the PTV $60\,Gy$ with weight of 100
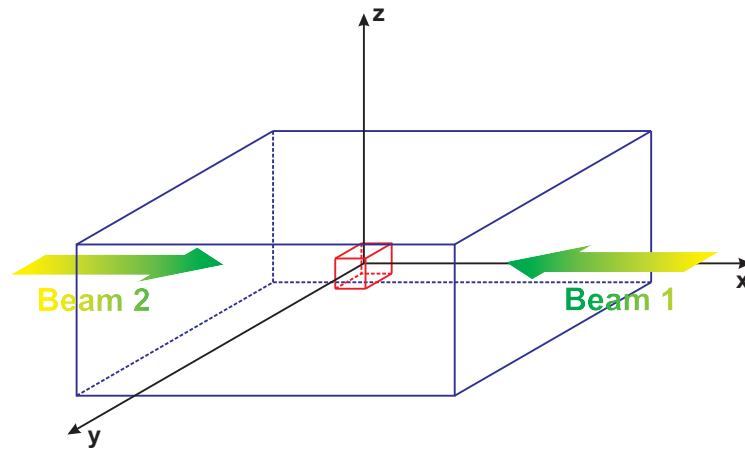
Figure 4.1.: Watertank (blue) with the PTV (red) in its center and the two opposing beams lying on the x-axis.

- Maximum Dose to the PTV 60 Gy with weight of 100

- Maximum Dose to the External (tank) 60 Gy weight of 5

- Dose Fall-Off of the External from 60 Gy to 0 Gy in 0.5 cm with weight of 5

Lastly, the energy layer spacing and the spot spacing were calculated by the automatic function of RayStation with scaling factors of 0.8 and 0.6, respectively. With a fixed target margin of 0.2 cm, this scaling factors showed the best results regarding dose conformity.

4.2. Treatment Plan for the Human Phantom

A CT-scan of a RANDO® (The Phantom Laboratory) phantom from the MATROSHKA experiment [24, 27, 28] was used in this thesis to create the treatment plan in RaySta-tion. This anthropomorphic phantom has no arms and legs, is based on a male torso and is built of tissue-equivalent polyurethane with embedded human skeleton. Its soft tissue has a density of $0.997\,g/cm^3$, the bones $1.3\,g/cm^3$ and the lungs $0.352\,g/cm^3$. The NUNDO (Numerical RANDO®) phantom [24, 25] (*Section 3.1*), which is a voxel transformation of the RANDO® with inbuilt organs and detectors, was used for the PHITS simulation.

The image set from the CT-scan consists of 175 slices, with a distance of 0.5 cm between each slice, which leads to a height of 87.5 cm. Some of the top and bottom slices had a bad quality or contained the base, the phantom was standing on, so the NUNDO has a total effective size of 84.5 cm.

The generic CT table was used to transfer the HU into mass density. On closer inspection it was found that the density displayed in RayStation slightly differs from the original density of the RANDO phantom. The soft tissue density in the TPS is of $1.02 - 1.04\,g/cm^3$ in RayStation instead of $0.997\,g/cm^3$ and the bones had a density of $1.3 - 1.8\,g/cm^3$ instead of $1.3\,g/cm^3$. This was no big problem, because the PHITS simulations were run twice with different densities and the difference in the dose deposition was negligible.

The PTV was defined in the Plan Design module with the same properties as in the watertank, a volume with the dimensions of $4 \times 4 \times 4\,cm^3$, placed at the back of the head (*Fig. (4.2)*). All other settings are the same as in *Section 4.1*, but now the isocenter of the PTV is located at (0.12, -6.5, 46.23) in the RayStation coordinate system and the external stands for the whole phantom in the objective/constraints section.

4.3. From RayStation to PHITS

The road from a treatment plan created in the RayStation TPS into an input file of PHITS is a little bit tricky, because each beam has its own coordinate system with the center in the isocenter and also the coordinate origin of the phantom was different in the TPS and in PHITS (the PHITS input file was adopted from [24, 25]), while the xyz-axes had the same direction.

RayStation exports the whole treatment plan including the image set into DICOM files. So it would be possible to use the DICOM2PHITS program to create the voxel body in PHITS and preserve the coordinate origin used in the TPS. But for the beams it is necessary to create the source in PHITS manually, because the beam information is not taken into account by DICOM2PHITS. Also the PTV and eventual ROIs have to be add manually.

DICOM2PHITS was not used in this work due to some reasons. First, for the watertank it is much easier to create just a simple box with homogeneous density instead of a detailed voxel geometry. This saves also a lot of computation time. On the other hand it was tried to use DICOM2PHITS for the phantom, but the attempt failed due to a too high resolution of the CT-scan. Instead, the NUNDO phantom was available, which is based on the same CT-scan and has also the advantage of its inbuilt organs and detectors. A disadvantage is that now the coordinate origin is different for the NUNDO phantom.

The DICOM output can only be read by some programs. For instance, the program

dicompyler visualizes the DICOM files and displays all information, like dose, beam parameters, spots, etc. The required information for the PHITS source section is the distance between the snout and the isocenter, the isocenter position, the spot positions, the spot size and the energy with the weighting factor of each spot. These parameters were read from the DICOM files by using the program *MATLAB* with its function *dicominfo* and afterwards, they were edited with a C++ program to match with the coordinate origin in PHITS.

Implementing the beam parameters into the PHITS source section was a little bit tricky. Each beam has its own three dimensional coordinate system with energy dependent layers defined by spot position, size and number of particles. First the easier implementation for the watertank is described and after that follows the more challenging one for the human phantom.

4.3.1. Export Procedure for the Watertank

The isocenter of the watertank was placed at the position (0,0,0) in the PHITS input file. The TPS coordinate system is shown for the human phantom in *Fig. (4.2)*. This figure applies also for the watertank. Thus, the beam has its own coordinate system with x'- and y'-axis, but one should not confuse it with the xyz-coordinate system in the TPS and in PHITS (*Fig. (4.2)*).

An example of the code in a PHITS input file for the first energy layer of the source is presented in A.1. Each energy layer has its own dumpfile with the following parameters in it:

Table 4.1.: The ID numbers in a dumpfile (A.1) of the source section of PHITS and their meaning.

number	meaning
1	particle type (e.g. protons)
2	x-position
3	y-position
4	z-position
9	weight
8	energy

The origin of the beam is determined by the x-, y-, z-position and *dir*, *phi* and *dom* (*Fig. (4.3)*) are the parameters determining the propagation and spread out of the
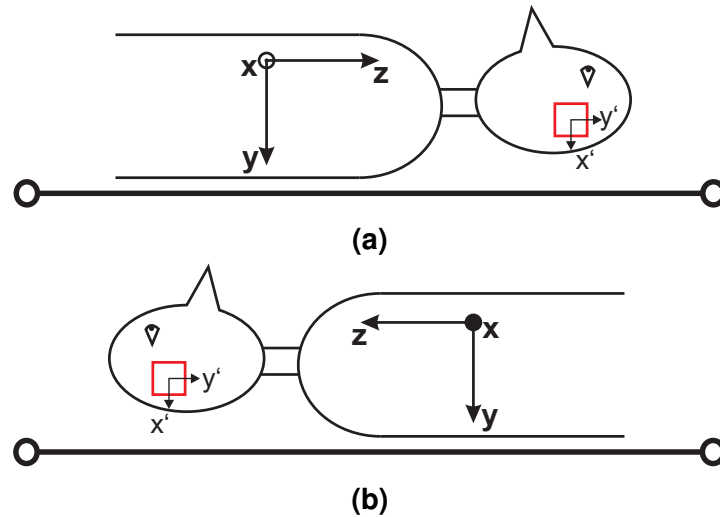
Figure 4.2.: Simplified sketch of the phantom lying on the treatment table (the table is not part of the simulation) and rotated over 180° on the z-axis from (a) to (b). The xyz-coordinate system belongs to the phantom and the xyz-axes have the same directions in the TPS and in PHITS, but they have a different origin of the coordinate system. On the other hand, the small x'y'-coordinate system with its origin in the center of the PTV (red) belongs to the beam. (a) Beams eye view of Beam 1 with positive x-axis (from xyz) coming out of the figure. (b) Beams eye view of Beam 2 with positive x-axis going into the figure.

beam. Hence, following from the coordinate systems in *Fig. (4.2a)* the first beam starts at $x = 64.8$ cm (distance snout→ isocenter) and flies towards the negative x-axis. The x'-value of the beam is assigned to the y-value of the phantom and the y'-value of the beam is assigned to the z-value of the phantom.

For the second beam, which comes from the opposing direction, *phi* has to be changed to 0 and the beam starts at $x = -64.8$ cm. Another difference is that the y'-value of the beam is now assigned to the minus z-value according to *Fig. (4.2b)*.

The *dom* parameter, which determines the spread out of the beam, is calculated in the following manner

$$\Psi = \arctan\left(\frac{\frac{spot\ size}{2}}{distance\ snout \rightarrow isocenter}\right) \quad (4.1)$$

according to *Fig. (4.3)* and the spot size varies between 8.4 and 8.9 mm.

The energy is constant for each energy layer
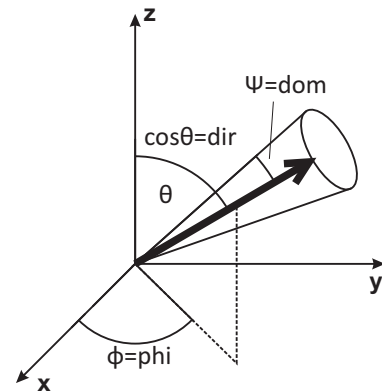
Figure 4.3.: The source parameters in PHITS *dir* and *phi* define the direction and *dom* the spread out of the beam (big arrow).

and the weight is the number of particles per spot.

4.3.2. Export Procedure for the Human Phantom

As mentioned before, the coordinate origin for the NUNDO phantom in PHITS and the RANDO® phantom in RayStation is different (*Fig. (4.4a)*). Hence, the biggest problem was to find the isocenter in PHITS. The other procedure was the same as for the watertank.

For simplification, the coordinate system of the organ shielding program (indicated in blue in *Fig. (4.4a)*) (*Section 3*) was used. When the coordinate origin of the shielding program is located at (0,0,0) then the origin in PHITS is shifted to (17.9,13.5,42.5).

The first step to determine the isocenter position in PHITS was to find the same slice in which the isocenter is located. In RayStation this slice has the z-position at 46.225 cm, which corresponds to $z = 77$ cm in the shielding program. The next step was to measure the distance between the isocenter and the outermost points of the phantom (*Fig. (4.4b)* and *Tab. (4.2)*) with the program *dicompyler*.

Table 4.2.: Outermost points in the x- and y-direction and their distance in the slice of the isocenter.

	x [cm]	y [cm]	distance x [cm]	distance y [cm]
RayStation	-7.6 → 8	-7.93 → 12.36	15.6	20.3
shieliding program	10.4 → 26	1.3 → 21.7	15.6	20.4

Afterwards these distances were used to find the isocenter in the shielding program coordinates, by subtracting or adding these distances to the outermost points of in the shielding program relative to the isocenter position in RayStation (0.12,6.5,46.225). Because the distances are not exactly equal in *Tab. (4.2)*, the mean value of the subtraction and summation was taken:

$$\text{x-direction:} \quad \left.\begin{array}{l} 10.4 + 7.6 + 0.12 = 18.12 \\ 26 - 8 + 0.12 = 18.12 \end{array}\right\} = 18.12$$

$$\text{y-direction:} \quad \left.\begin{array}{l} 1.3 + 7.93 + 6.5 = 15.73 \\ 21.7 - 12.36 + 6.5 = 15.84 \end{array}\right\} = 15.785$$
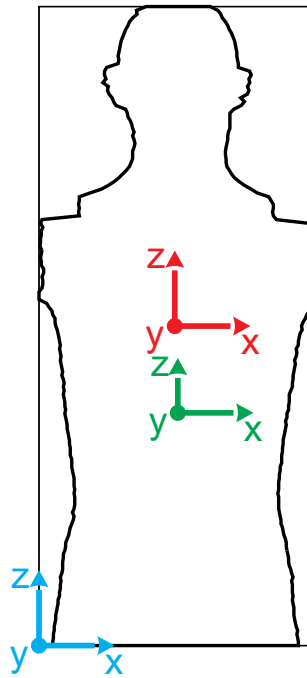
(a) Front view of the phantom with coordinate origin in PHITS (red), RayStation (green) and the shielding program (blue).
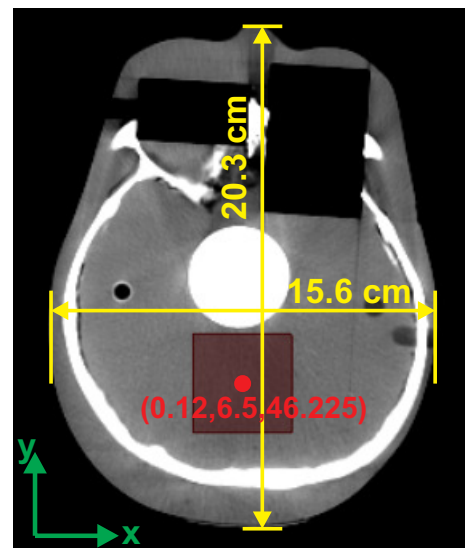
(b) The slice of phantom in which the isocenter (red point) is located with the distances towards the borders in x- and y-direction. The dark red box represents the PTV.

Figure 4.4.

This leads to the position of the isocenter at (18.12,15.785,77) in the shielding program. The last step was to switch into the coordinates system of PHITS by subtracting (17.9,13.5,42.5), which leads to final coordinates of the isocenter located at (0.22,2.285,34.5) in PHITS.

Now follows the same procedure as for the watertank by creating the source section with the dumpfiles in PHITS, but the x-, y- and z-parameters in the dumpfiles, which determine the start position of the beam, need a correction, because the isocenter is not at (0,0,0). Hence, the first beam starts at x = (64.8 + 0.22) cm = 65.02 cm and the second beam at x = (−64.8 + 0.22) cm = −64.58 cm. According to *Fig. (4.2)*, one has to add 6.5 cm to the y-parameter and 34.5 cm to the z-parameter for both beams. The spot size for the human phantom varies between 11.5 and 16.3 mm.

Finally, the transfer of the treatment plan from RayStation to PHITS is finished. The only thing that is missing, is to define the PHITS input file, which will be explained in the next chapter.

4.4. PHITS Input File

The basic structure of a PHITS input file was explained earlier in *Section 2.4.1*. As in the previous chapters, the input file for the watertank will be described first and then follows the more complex one for the human phantom.

4.4.1. Input File for the Watertank

A total number of 100 million particles (5000 particles per batch times 20000 batches) was chosen to get a good accuracy in a reasonable time. An energy cut-off was set for protons, neutrons, electrons, positrons and photons. The INCL model (*Section 2.4.2*) for nucleon (proton and neutron), pion and light ion (up to ^{4}He) induced reaction was used combined with the GEM model for the de-excitation phase of the particles. Also the improved version 2 of the event generator was used.

Two models for multiple Coulomb scattering (MCS) and energy straggling were tested. Once with Lynch's formula based on the Moliere theory for MCS and Landau Vavilov distributions for energy straggling and the other time with the ATIMA code (*Section 2.4.2*). Both approaches brought good results, but ATIMA shows an advantage (*Section 5*).

The source section of the input file was described above in *Section 4.3*. As the name

implies, the material of the watertank is water (H_2O) with a density of $1.02\,g/cm^3$ surrounded by air with a density of $1.21 \cdot 10^{-3}\,g/cm^3$. Normally the density of water is $1\,g/cm^3$, but $1.02\,g/cm^3$ was adopted from RayStation.

As mentioned in *Section 4.1* the watertank is a simple box with a size of $50 \times 50 \times 20\,cm^3$, where the PTV, a cubic box ($4 \times 4 \times 4\,cm^3$), is located in the center.

The main goal of the watertank simulations was to compare the dose in the PTV calculated by RayStation with the dose simulated in PHITS. Hence, the first tally was [t-heat], in which the absorbed dose deposited in the PTV and also in the whole tank was measured. Another [t-heat] tally was used for a more detailed investigation of the dose deposition in a $2\,mm$ thick slice through the center of the PTV in the xy-plane with a resolution of $4\,mm^2$ per cell and one with a $4\,cm$ thick slice, which covered the whole PTV. The last three tallies measured the line doses in x-, y- and z-direction in a $1\,mm^2$ small area through the watertank.

This simulation was carried out on the ATI 64 core server, which runs on Windows Server 2008 and it took about 8 days with 30 cores.

4.4.2. Input File for the Human Phantom

Except for the number of particles, the parameter settings in the input file of the phantom were kept the same as for the watertank. Because the most distant detectors in the phantom were almost $80\,cm$ away from the incoming beams, only very few particles arrived there. So it was necessary to simulate a lot of particles to get a good accuracy in the more distant detectors. The total number of particles was set to 800 million, which takes a lot of calculation time. This could not be achieved on the ATI server in a reasonable time, so the simulation was performed on a fast Linux server in Sweden using 64 cores.

Due to a bug at the Linux compiled PHITS version, ATIMA code reported unexpected failure, so Lynch's formula and Landau Vavilov distributions were used instead. To compare the results in the region around the PTV, ATIMA was used on the ATI server but only with about 180 million particles.

The NUNDO phantom consists of the materials listed in *Tab. (4.3)* with their composition. Water was used for the TLDs instead of their original material, as the measured dose in experiments is always calibrated to water.

As mentioned in *Section 4.2*, the density of the soft tissue and the bones were changed to $1.03\,g/cm^3$ and $1.6\,g/cm^3$ instead of $0.997\,g/cm^3$ and $1.3\,g/cm^3$, respectively,

Table 4.3.: Materials of the NUNDO phantom

Material	Element	Weight	Material	Element	Weight
Soft Tissue	Hydrogen	0.0918	Bones	Hydrogen	0.07
	Carbon	0.6778		Carbon	0.345
	Nitrogen	0.0250		Nitrogen	0.028
	Oxygen	0.2031		Oxygen	0.368
	Antimony	0.0022		Sodium	0.001
Lungs	Hydrogen	0.0597		Magnesium	0.001
	Carbon	0.7074		Phosphorus	0.055
	Nitrogen	0.0190		Sulfur	0.001
	Oxygen	0.2128		Calcium	0.129
	Antimony	0.0010	Air	Hydrogen	0.0006
				Nitrogen	0.754
				Oxygen	0.2326
				Argon	0.0128

due to differences caused by the generic CT table, so that the results of the simulation are comparable to the calculation in RayStation. But the effect in the dose due to this change was negligible.

The voxel file (*Section 3.1*), which contains the information about the NUNDO phantom, was imported to PHITS by setting *ivoxel* = 2 in the parameter section. This function converts the voxel file into a binary file, which is further used for the simulation. To convert the file properly, the cell and surface section of PHITS have to be defined in the following manner.
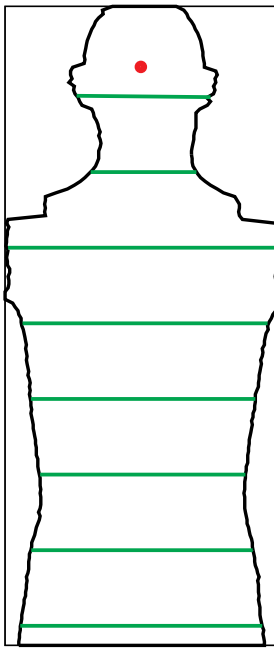
In the surface section, only the rectangular shaped voxels ($1 \times 1 \times 5\,mm^3$) and the cuboid ($35.8 \times 27 \times 84.5\,cm^3$), which contains the whole phantom with the surrounding air, were defined. It is helpful to use the *lattice* and *universe* functions in PHITS for voxel phantoms. Each organ, each TLD and the air got their own universe assigned in the cell section. Then a lattice with 358 points in x-, 270 in y- and 169 in z-direction (according to the voxel file in *Section 3.1*) were filled with these universes. After the creation of the binary voxel file, *ivoxel* was set to 1 for the simulation.

The contribution of neutrons and photons to the dose was of interest, but to observe these particles the counter section had to be included in the input file. Every time when these particle collide, they deposit energy and thereby it was possible to measure only the dose produced by them.

There were only two types of tallies written in the input file. The first type measured the dose of a specific region and the other one the fluence. The dose was measured in

all organs, the ptv and all TLDs. For each of these regions three tallies were set. One observed the absorbed dose deposited by all particles, one only the dose deposited by neutrons-secondaries and the last one only the dose deposited by photons.

A more detailed investigation of the dose in the area around the PTV was performed by observing ten 1 cm thick slices in the xy-plane with a resolution of $1\,mm^2$ per cell and one 4 cm thick slice, which covered the whole PTV. To observe line doses, the deposited energy in the x-,y- and z-direction through a $1\,mm^2$ small area, penetrating the phantom through the center of the PTV was measured.

Because it is interesting to know how far and how many particles travel through the phantom, the tally [t-cross] was implemented. Rectangular surfaces in the xy-plane were created, to count the particles crossing each area (*Fig. (4.5)*). The first surface was 4.5 cm away from to the isocenter in the z-direction, while the other ones have a distance of 10 cm to each other.

The fluence of protons, neutrons, photons and all particles was observed in all surfaces in the unit *number of particles per mm^2*. Also their energy range was measured in 10 MeV steps from 0 to 150 MeV.

Figure 4.5.: [t-cross] tallies count protons, neutrons and photons crossing the green surfaces.

4.5. Data Evaluation

PHITS calculates the dose in the unit *MeV/Source*, so this unit has to be transferred into $Gy = J/kg$. The conversion factor from the energy E in MeV to Jule is the following: $1MeV = 1.60218 \cdot 10^{-13} J$. *Source* is the total number of particles N from both beams and it was read out from the DICOM files of the treatment plan. To get the mass m one needs the volume V and the density ρ of the region in which the dose was calculated.

$$D = \frac{1.60218 \cdot 10^{-13} \cdot E \cdot N}{V \cdot \rho} = \frac{1.60218 \cdot 10^{-13} \cdot E \cdot N}{m} \tag{4.2}$$

The graphic utility *gnuplot* was used to present the data in figures in *Section 5*. But

the output files from PHITS are not so handy, so some C++ programs were written for every tally to rewrite the output files into files which are easier readable for *gnuplot*. Also some parts of the shielding program (*Section 3.2*) were used to enable a 3D-presentation of the phantom with all TLDs including their doses inside.

5. Results

This chapter presents the results of this study and is separated into two sub chapters. At first the results for the watertank are presented, including a comparison of the doses from RayStation and PHITS deposited in the PTV, a detailed investigation of the dose in and around the PTV, a comparison of the results by using Lynch's formula and the Landau Vavilov model or the ATIMA code for angular (MCS) and energy straggling in PHITS and a look on the line doses in x-, y- and z-direction through the PTV.

In *Section 5.2* the results for the human phantom, which can be used for future experiments at the MedAustron and for an estimation of the risk of secondary cancers, are presented. The data are presented in the same way as for the watertank and in addition a detailed investigation of the deposited dose in the organs and in the TLDs is made, with a consideration of the dose deposited by neutrons and photons.

5.1. Watertank

Tab. (5.1) shows the absorbed doses calculated by RayStation and PHITS for the watertank. D50 is the minimum dose at 50 % of the volume of the PTV and Av stands for the average dose. The PHITS simulations were ran twice, once with Lynch's formula and Landau Vavilov distributions and once with the ATIMA code for angular and energy straggling. For simplification Lynch's formula and Landau Vavilov distributions will further be called Lynch.

Table 5.1.: Absorbed dose in the PTV of the watertank calculated by RayStation and PHITS.

		Dose [Gy]
RayStation	Av	59.95
	D50	59.92
PHITS	Lynch	62.93
	ATIMA	59.51

The PHITS simulation with ATIMA shows a very good agreement within 1 %,

comparing to results obtained with RayStation for the dose in the PTV. The results with Lynch are within 5 %.

The doses for the following figures, for a detailed investigation of the dose deposition in and around the PTV, are scaled to the prescribed dose of 60 Gy=100 % and displayed in percent of the prescribed dose. *Fig. (5.1)* shows a comparison between the results of ATIMA and Lynch for the deposited dose in and around the PTV. The PTV is fully covered in z-direction. ATIMA delivers a more homogeneous dose inside the

(a)

(b)

Figure 5.1.: Comparison of doses simulated by ATIMA (a) and Lynch (b) in and around the PTV (black box). The z-axis (z=[-2:2]=4 cm) covers the whole PTV. It is shown that the dose deposition of ATIMA is more homogeneous inside the PTV and overall lower than those from Lynch.

PTV than Lynch with values from 90 % to 110 % of the prescribed dose, while Lynch

exceeds 130 % in some areas. The dose from RayStation was always below 110 %. Furthermore the dose from ATIMA outside of the PTV is slightly lower. Besides the comparison of ATIMA and Lynch, the incoming beams are divided into four stripes and the dose in the entrance of the first stripe (y=1.9 cm) is pretty high (around 90 %) for both beams. There is also a sharp lateral dose fall-off to less than 10 % after 1.3 cm beyond the PTV.

Fig. (5.2) shows only a small 2 mm thick slice through the center of the watertank and allows a direct comparison with the dose calculated by RayStation (*Fig. (5.2c)*). Also the color range of the dose has now discrete values. While ATIMA shows a similar distribution of the dose as in *Fig. (5.1a)*, the difference to Lynch is even more apparent, where the dose reaches values down to 80 % and up to 150 % in some areas inside the PTV.

The comparison between PHITS and RayStation shows that the dose outside the PTV from PHITS is almost everywhere lower, except for the first stripe (y=1.9 cm) where the dose is higher. In *Fig. (5.2a)* there is a high dose regime at the right side of the PTV up to 120 % which is not present in *Fig. (5.2c)*. As mentioned before, the absorbed dose calculated by RayStation is everywhere below 110 %. ATIMA reproduces the dose distribution from RayStation, due to a lower maximum dose in the PTV, better than Lynch, but not accurate.

An advantage of PHITS compared with RayStation is, that it is possible to observe very small doses, which is shown in *Fig. (5.3)* where the dose distribution in the watertank in an 1 cm thick slice up to 10^{-4} % is presented. Next to the high dose region of the incoming beams, there is a few centimeter thick region with a dose below 1 % (yellow). After that the doses are very low until the dose reaches values below 10^{-3} % of the prescribed dose at y = ±20 cm.

As shown in *Fig. (5.2)* there are some discrepancies regarding the dose distribution between RayStation and PHITS. Line doses (calculated with ATIMA) through the center of the PTV in x-, y- and z-direction allow a more detailed investigation (*Fig. (5.4)*). There are differences between PHITS and RayStation inside the PTV in all directions. While the PHITS dose varies between 60 Gy and 70 Gy in x-direction, the PHITS doses in y- and z-direction are pretty constant at around 58 Gy. RayStation delivers constant doses of 60 Gy in all directions. The dose-fall off matches perfectly in y- and z-direction, but in x-direction PHITS calculates lower doses than RayStation and the difference rises with distance, which was also observed in *Fig. (5.2)*.

In conclusion it was shown that PHITS is able to reproduce the average dose in
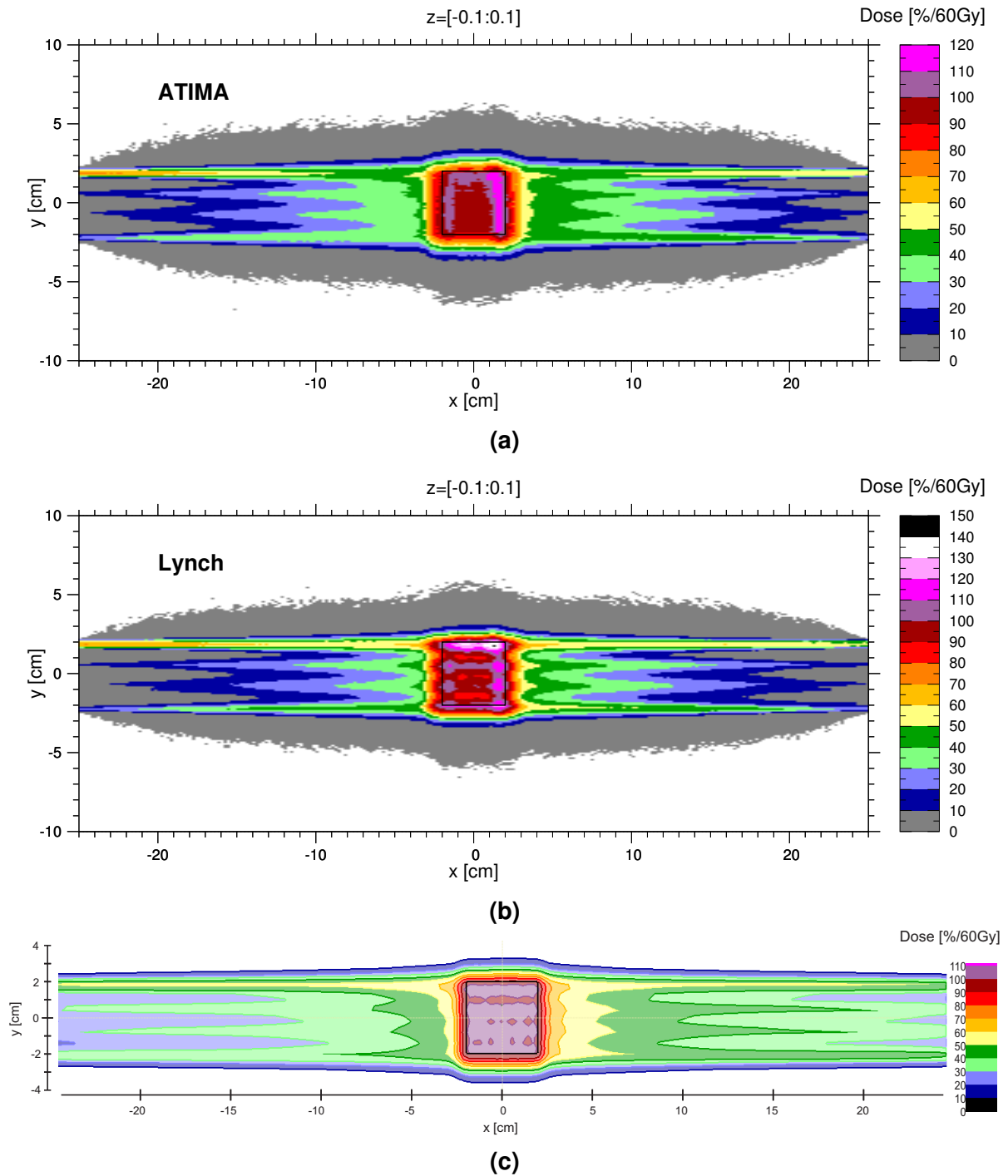
Figure 5.2.: Comparison of doses simulated by ATIMA (a), Lynch (b) and RayStation (c) in and around the PTV (black box). The z-axis (z=[-0.1:0.1]=2 mm) covers only a small slice through the watertank. (c) was observed directly from RayStation 5 and the dose between 0 and 10 % is ignored.
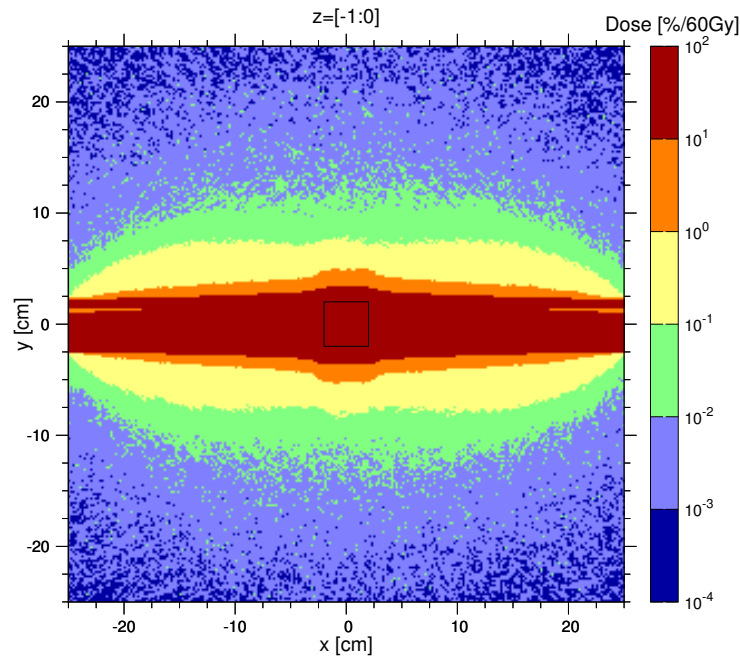
Figure 5.3.: Dose distribution in the whole watertank up to 10^{-4} % of the prescribed dose. The z-axis (z=[-1:0]=1 cm) covers a small slice through the center of the watertank.
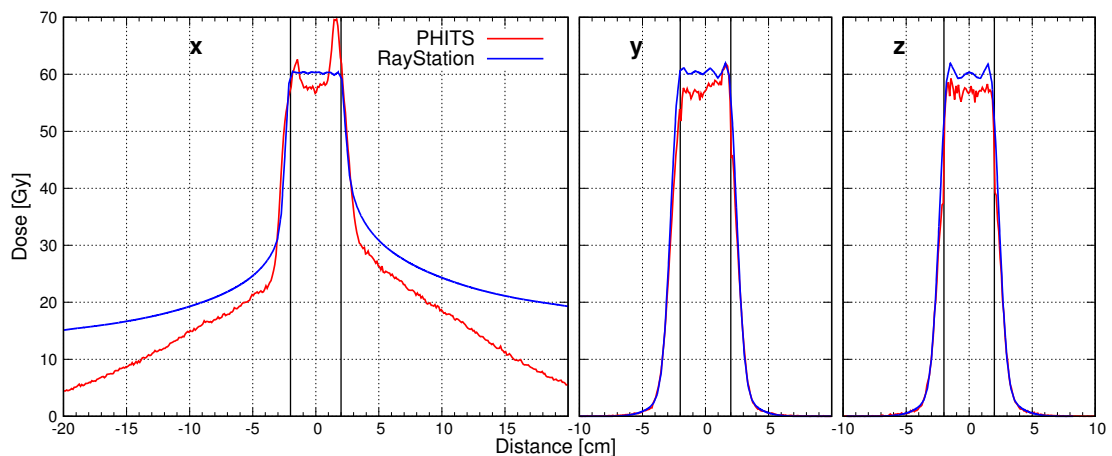
Figure 5.4.: Line doses calculated by PHITS and RayStation through the center of the PTV in x-, y- and z-direction. The vertical black lines at ±2 cm indicate the border of the PTV.

the PTV from a treatment plan from RayStation. ATIMA is a better model for MCS and energy straggling than Lynch, especially for a detailed investigation of the dose distribution, but the detailed dose distribution from PHITS inside and outside the PTV was not satisfying.

5.2. Human Phantom

5.2.1. Absorbed Dose in the PTV

Different to the watertank, Lynch shows a slightly better agreement with RayStation for the absorbed dose in the PTV of the phantom than ATIMA (*Tab. (5.2)*). Lynch has a 1 % and ATIMA a 3 % difference to the dose from RayStation. There are some factors which can explain the difference with respect to the results for the watertank (ATIMA had a very good agreement in *Section 5.1*). First, RayStation used a CT-scan of a RANDO phantom, while PHITS used the NUNDO phantom and they do not have the exact same geometry. Another point is that the mass density in PHITS

Table 5.2.: Absorbed dose in the PTV of the phantom calculated by RayStation and PHITS.

|		Dose [Gy]
RayStation	Av	59.99
	D50	59.95
PHITS	Lynch	60.64
	ATIMA	58.15

was homogeneous for the tissue and the bones. The mass density in RayStation was calculated from the CT-scan and is only approximately homogeneous (tissue density $1.02 - 1.04 \, g/cm^3$, bones density $1.3 - 1.8 \, g/cm^3$ in the head). Concerning the mentioned differences, the results are pretty good.

Despite ATIMA delivered better results for the watertank, it will only be taken into account in *Section 5.2.2* for a detailed investigation of the dose distribution in and around the PTV. Lynch will be used in the other following sections, due to better statistics.

5.2.2. Dose Distribution in and around the PTV

The comparison of the deposited dose in the whole PTV from ATIMA and Lynch in *Fig. (5.5)* provides similar results as for the watertank. ATIMA delivers values between 80 % and 110 %, while Lynch exceeds 130 % of the prescribed dose inside the PTV in some areas. Both have in common that there are four stripes of high doses, separated by three stripes of lower doses inside the PTV.

A difference is that high doses occur at the top left and at the bottom right outside of the PTV by ATIMA, which does not apply for Lynch where the high dose is mostly
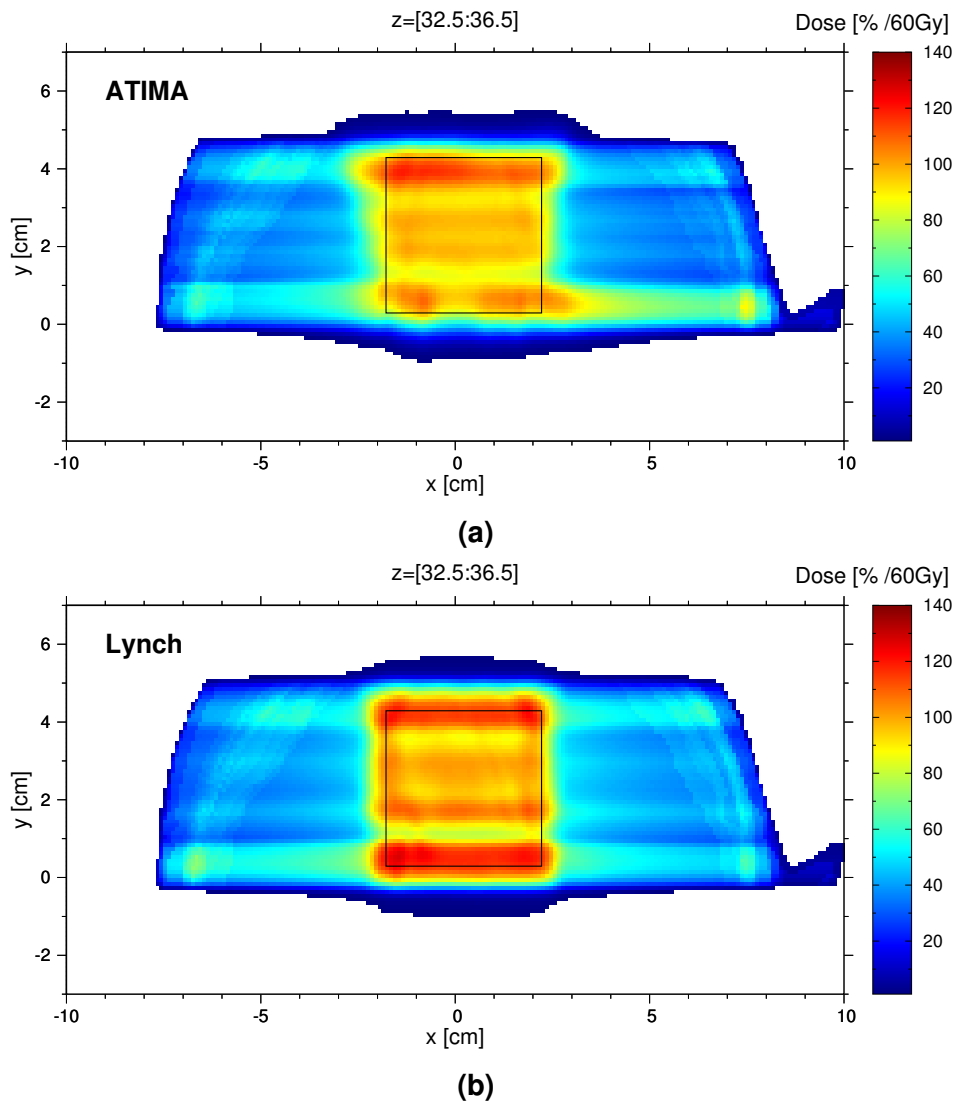
Figure 5.5.: Comparison of the dose distribution simulated by ATIMA (a) and Lynch (b) in and around the PTV (black box). The z-axis (z=[32.5:36.5]=4 cm) covers the whole PTV. The bones are visible, because the whole dose was calculated with the density of the tissue, which results in a 60 % higher dose for the bones.

inside and a few millimeter above and below the PTV. It is also interesting, that the bottom beam stripe (y = 0-1 cm) shows a pretty high dose on the right site for ATIMA but on the left side for Lynch. It has to be considered that the doses for the bones are 1.6 times to high, because all doses were calculated with the density of the tissue. This applies also for the following figures.

A closer look on a 1 cm thick slice through the center of the PTV in *Fig. (5.6)* enables a comparison with the dose distribution calculated by RayStation (*Fig. (5.6c)*). It can be seen that neither ATIMA nor Lynch can reproduce the result from RayStation very

accurate. Both types show advantages and disadvantages against the other. Discrepancies were also seen for the watertank and are reinforced due to some geometry
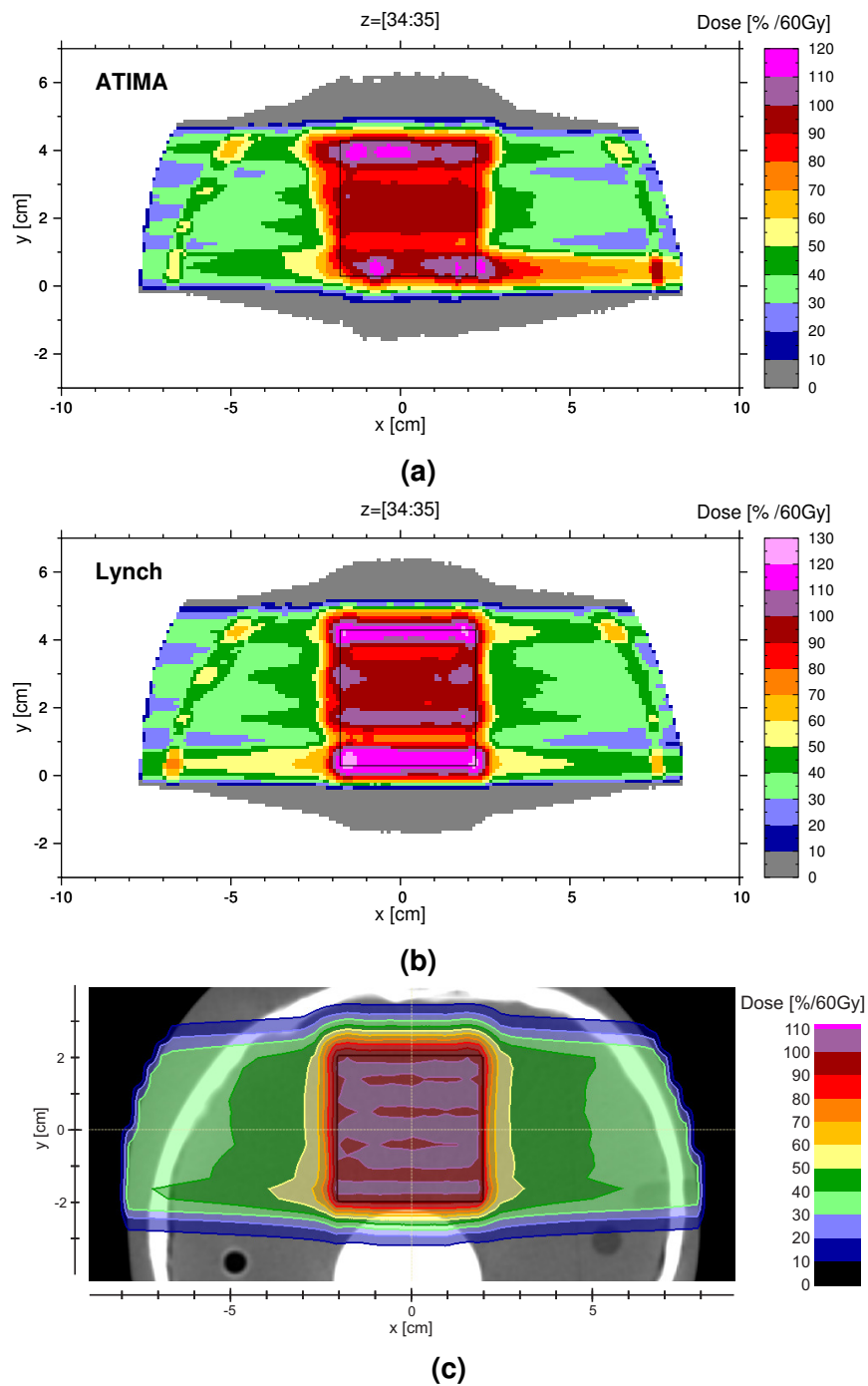

(a)

(b)

(c)

Figure 5.6.: Comparison of the dose distribution simulated by ATIMA (a), Lynch (b) and RayStation (c) in and around the PTV (black box). The z-axis (z=[34:35]=1 cm) covers a slice through the center of the PTV. (c) The white circle indicates the holder of the phantom.

differences between RANDO and NUNDO, an inhomogeneous density distribution in RayStation and overall the phantom has a more complex structure and material composition than the watertank.

(a)

(b)

(c)
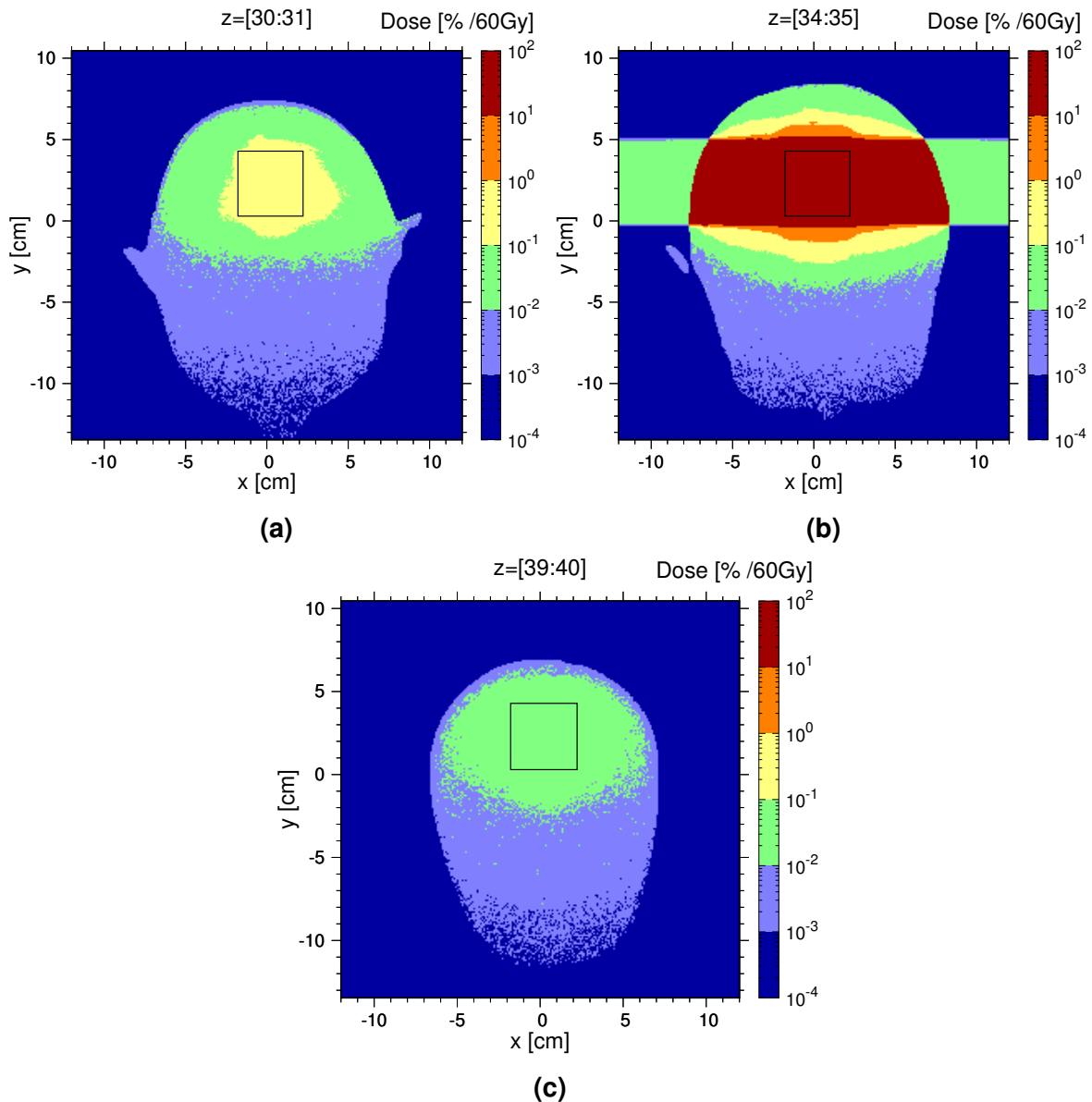
Figure 5.7.: Dose distribution from Lynch in the area around the PTV of the phantom up to 10^{-4} % in different 1 cm thick slices. The PTV (black box) covers the area between $z = 32.5$ cm to $z = 36.5$ cm. (b) The dose generated by the incoming beams in the air outside of the phantom is about 1000 times to high, because the dose was calculated with the density of tissue instead of air.

Because the simulation with Lynch had better statistics due to more particles, the results from Lynch are used in *Fig. (5.7)* for a detailed look on the dose distribution in

the area around the PTV up to 10^{-4} % of the prescribed dose. *Fig. (5.7b)* shows the dose distribution through the center of the PTV. There is a sharp lateral dose fall-off next to the region of the incoming beams. At the front of the phantom head (y = -10 cm) the dose reaches very low values below 10^{-3} %.

The dose fall-off a few centimeter outside the PTV is approximately isotropic in y- and z-direction, shown in *Fig. (5.7a)* and *Fig. (5.7c)*, but it seems, at least up to 4 cm distant to the PTV in z-direction, that the dose further away from the PTV at y = -10 cm is independent from the z-distance.

5.2.3. Line Doses
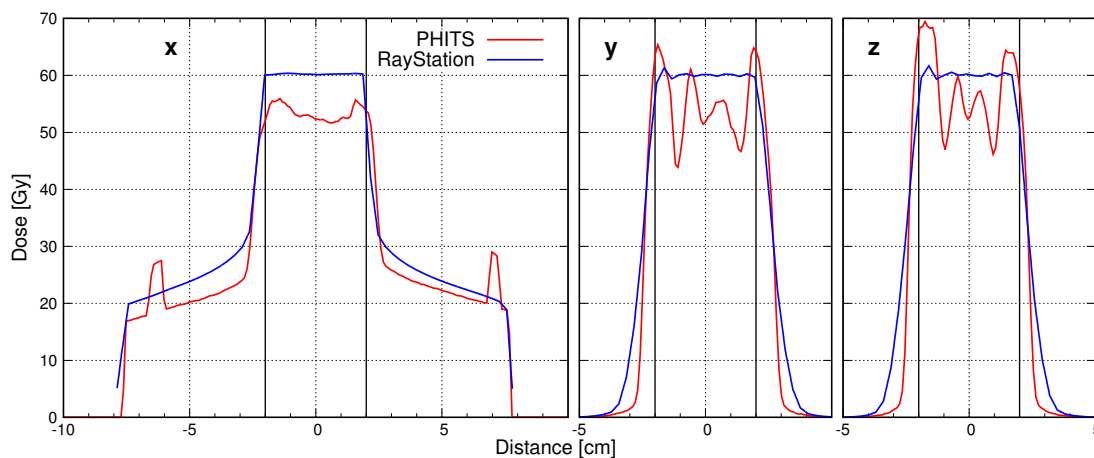
Figure 5.8.: Line doses calculated by PHITS and RayStation through the center of the PTV in x-, y- and z-direction. The vertical black lines at ±2 cm indicate the border of the PTV. The peaks in **x** at ±7 cm indicate the bones, which were calculated with the tissue density.

As it was shown in *Fig. (5.6)*, PHITS was not able to reproduce the dose deposition in and around the PTV very accurate from RayStation. This is also observed in the line doses through the center of the PTV in x-, y- and z-direction (*Fig. (5.8)*). The line doses from RayStation are pretty smooth in all directions, which does not apply for those from PHITS. In y- and z-direction the dose inside the PTV shows strong fluctuations around 60 Gy and also the dose fall-off does not match exactly as it did in the watertank. This fluctuations were also observed in *Fig. (5.5)* and *Fig. (5.6)* with four stripes of high doses, separated by three stripes of lower doses inside the PTV. The x line dose from PHITS is always a few Grays lower than that from RayStation (except for the peaks at ±7 cm, which indicate the bones, which were calculated with the tissue density).

5.2.4. Organ Doses

Tab. (5.3) lists the organs of the NUNDO phantom together with the absorbed dose (ordered by size), the dose only from neutrons and photons and a mean distance. The mean distance is inappropriate for some organs, which are widely spread in the body, like bones, skin, remainder and red bone marrow, and should be ignored for them. First the absorbed doses will be discussed and then the portion of the absorbed dose only produced by neutrons and photons will be investigated.

The dose received by the PTV was discussed earlier in *Section 5.2.2.* Only the dose for the brain was also calculated by RayStation, the doses for the other organs are too low for a consideration by RayStation. A average dose of 12.82 Gy was the result from RayStation in the brain, but PHITS got only 9.64 Gy, which makes a difference of about 25 %. This difference was probably caused, next to the previous mentioned differences from RANDO and NUNDO, by the holder (white circle in *Fig. (5.6c)*) and holes in the CT-images of the phantom. Another point is, that the brain was generated automatically in RayStation and thus, there should be geometrical differences with the brain of the NUNDO phantom.

High doses were also received by the bones, the skin and the remainder. These high doses are mainly produced in the area of the incoming beams, so it would have been better to separate these organs into two regions, to observe more meaningful values. One region would be the head, which receives the high doses and the other region would receive a significant lower dose.

The dose received from the remaining organs decreases with increasing mean distance to the PTV, which was expected. Organs near to the PTV, like tongue and eyes, received doses in the mGy area, while the testes, which are the most distant organ, received a dose of just 2 μGy.

The dose contribution from neutrons and photons in *Tab. (5.3)* are presented in percent of the absorbed dose. It is conspicuous that the sum of both adds up to about 110 % of the absorbed dose for most organs outside the beam line. This should not be possible, because 100 % should be the maximum, but there are two possible explanations for this behavior. First the uncertainties of the doses in each tally could cause this behavior. For instance, the relative error for the tongue lies between 1 and 2 % for each tally, but neutron and photons still add up to 105 %. Hence, the uncertainties do not cause this behavior. A more satisfying explanation is the following. Every time when a neutron or a photon interact with matter, there is a possibility that they undergo nuclear reactions, in which new neutrons or photons are

Table 5.3.: Organs of the NUNDO phantom with the absorbed dose ordered by size. The neutron and the photon doses are presented in percent of the absorbed dose. The mean distance of the organs to the isocenter of PTV can be found in the last column.

organ	absorbed dose [Gy]	neutron [%]	photon [%]	distance [cm]
PTV	$6.06 \cdot 10^1$	0.05	0.01	0
brain	9.64	0.11	0.02	5.593
bones	$2.89 \cdot 10^{-1}$	0.33	0.11	35.86
skin	$1.78 \cdot 10^{-1}$	0.22	0.07	41.68
remainder	$2.28 \cdot 10^{-2}$	0.75	0.28	47.79
salivary glands	$1.34 \cdot 10^{-3}$	73.21	26.00	12.34
tongue	$1.18 \cdot 10^{-3}$	75.53	30.16	12.04
eyes	$7.47 \cdot 10^{-4}$	73.48	33.04	13.17
eye lense	$5.85 \cdot 10^{-4}$	70.04	36.13	13.95
red bone marrow	$4.40 \cdot 10^{-4}$	29.11	10.93	52.99
oesophagus	$3.63 \cdot 10^{-4}$	73.84	33.00	27.1
thyroid	$3.39 \cdot 10^{-4}$	67.32	41.10	17.76
trachea	$2.36 \cdot 10^{-4}$	66.14	42.40	20.8
spinal cord	$8.66 \cdot 10^{-5}$	66.98	40.73	46.39
lungs	$6.90 \cdot 10^{-5}$	59.34	49.57	33.45
thymus	$6.47 \cdot 10^{-5}$	60.68	49.22	30.52
breast	$3.58 \cdot 10^{-5}$	57.06	52.95	37.47
heart	$3.31 \cdot 10^{-5}$	58.21	52.75	39.98
spleen	$2.06 \cdot 10^{-5}$	55.10	54.62	49.34
stomach	$1.84 \cdot 10^{-5}$	55.99	55.88	48.91
liver	$1.71 \cdot 10^{-5}$	55.90	55.18	49.49
kidney	$1.06 \cdot 10^{-5}$	54.09	58.84	56.51
pancreas	$9.66 \cdot 10^{-6}$	52.35	61.72	56.12
gall-bladder	$9.37 \cdot 10^{-6}$	52.65	57.21	54.47
colon	$7.11 \cdot 10^{-6}$	51.91	60.40	62.14
small intestine	$6.76 \cdot 10^{-6}$	50.75	61.76	62.38
ovaries	$5.31 \cdot 10^{-6}$	42.02	66.31	66.04
rectum	$2.91 \cdot 10^{-6}$	48.28	65.74	73.48
prostate	$2.45 \cdot 10^{-6}$	44.80	65.73	76.46
bladder	$2.44 \cdot 10^{-6}$	33.86	77.13	74.49
testes	$1.99 \cdot 10^{-6}$	29.26	80.28	76.87

produced. So the dose from neutrons and photons may be counted more than once.

For all organs, which were penetrated by the incoming proton beams, the dose portion from neutrons and photons is negligible. On the other hand, the organs which were not in the beam line, receive their dose mainly from neutrons and photons. The dose of the organs closest to the PTV but outside the beam line, is produced largely by

neutrons. With increasing mean distance, the share of the neutrons to the absorbed dose decreases, while that of photons increases. At around 50 cm both shares are equal and with increasing distance, the dose from photons dominates.

5.2.5. TLD Doses

As mentioned in *Section 3.1*, the NUNDO phantom consists of 1596 TLDs which are placed in a regular grid. *Fig. (5.9)* shows a gross overview of the dose deposited in these detectors up to nGy. Starting from high doses near the PTV the dose decreases rapidly and is barely noticeable at the bottom of the phantom. A more detailed investigation of the doses in the TLDs will be given in the following.

Fig. (5.10a) shows the dose deposited in each detector and also the dose produced only by neutrons and photons with their dependence of the absolute distance to the isocenter. *Fig. (5.10b)* is similar and shows the portion of the absorbed dose by neutrons and photons in percent. There are large uncertainties with the values above 30 cm, shown in *Fig. (5.11)*, but it is still possible to recognize some patterns.

In the region around the PTV, the dose from protons clearly dominates, but after 5 cm the neutron dose contributes over 50 % to the absorbed dose and also the dose from photons contributes between 20 and 30 %. The 10 to 20 % of the absorbed dose between 5 and 10 cm, which are not generated by neutrons or photons are probably generated by protons and electrons, but above 10 cm almost all the dose is produced by neutrons and photons. Same as for the organ doses, neutrons dominate up to 40-50 cm and afterwards the dose from photons is dominating.

The values for the most distant detectors vary around μGy, which is consistent with the results of the most distant organs. Some detectors received also a dose in the nGy area, but this is affected by the large uncertainties. The relative errors from neutrons are considerably larger than those from photons as shown in *Fig. (5.11)*.

5.2.6. Fluence through the Phantom

This section investigates the fluence of protons, neutrons and photons through xy-planes of the phantom (*Fig. (4.5)*). The total number of particles per cm^2, their decrease rate with distance to the isocenter and their energy are presented.

Fig. (5.12) shows the amount of particles per cm^2 in dependence of the relative distance to the isocenter in z-direction for protons, neutrons and photons. They all decrease with increasing distance, approximately with a negative exponential
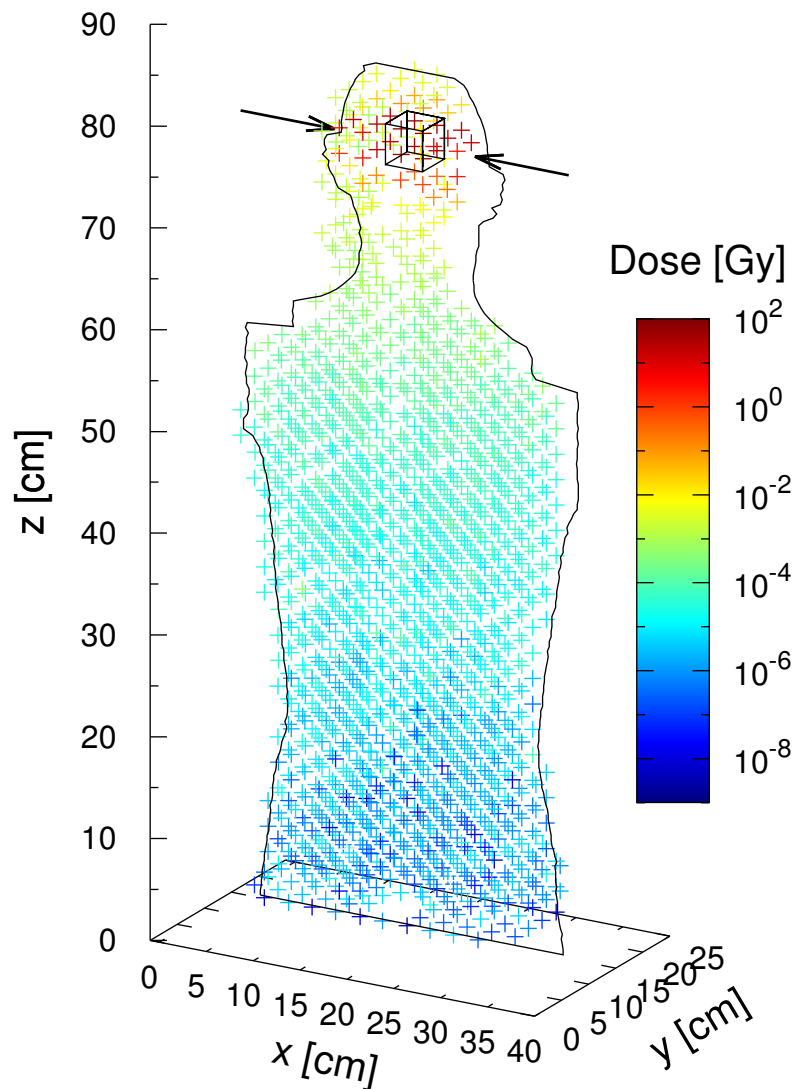
Figure 5.9.: All detectors in the phantom with their received dose up to 10^{-9} Gy. The shape of the phantom, the incoming beams and the PTV are indicated.

slope. Photons show the slowest decrease rate with about two magnitudes over the whole phantom while neutrons have three magnitudes. Protons are negligible after 20 cm where just about 100 particles/cm^2 are observed and only one particle/cm^2 was measured in the last xy-plane. This results were expected, because protons possess a charge and thus interact much more with matter than the uncharged neutrons and photons.

Fig. (5.13) allows also the observation of the energy of these particles. The only

(a)

(b)
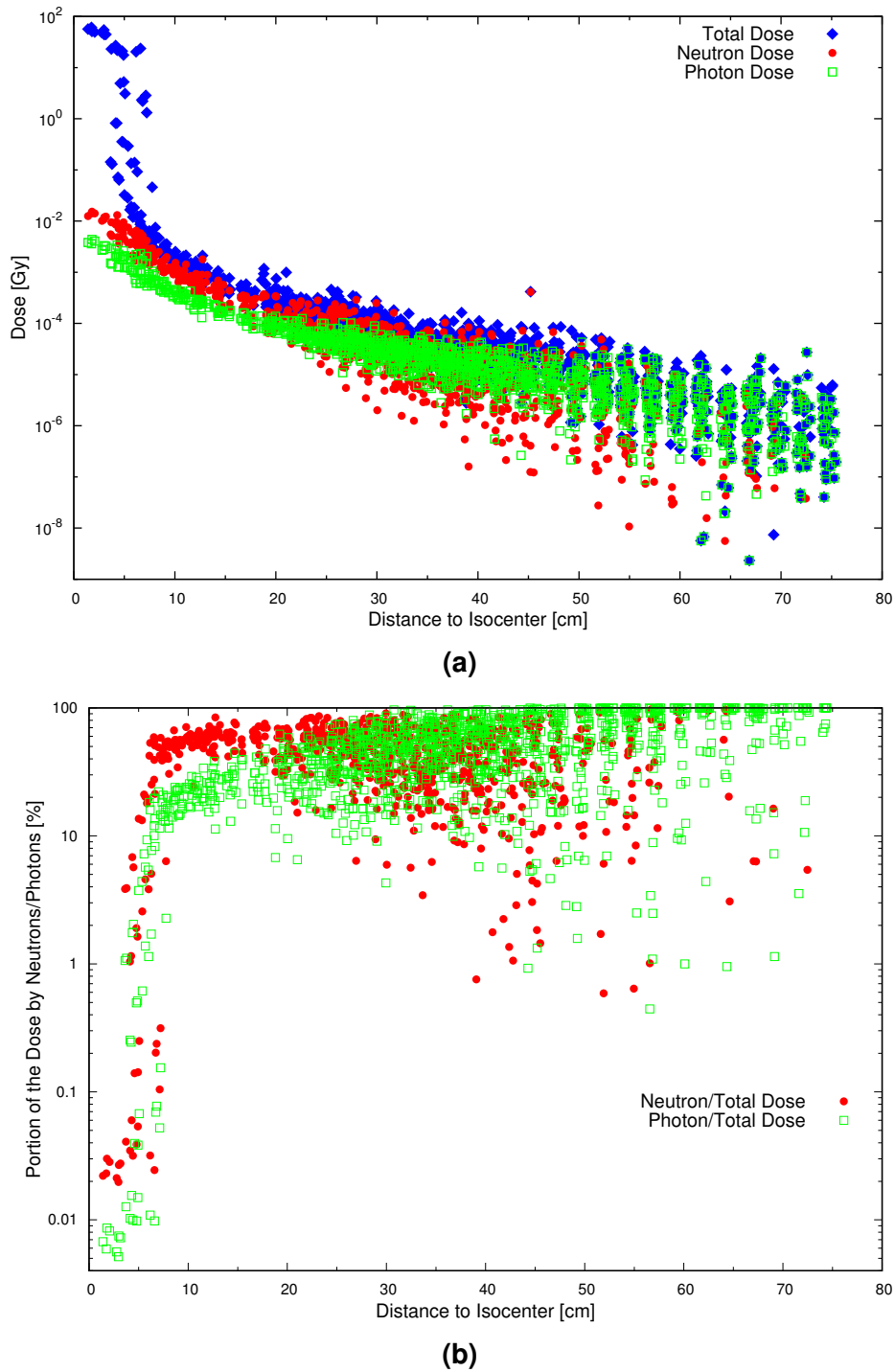
Figure 5.10.: (a) Dose deposited in each detector with the absolute distance to the isocenter of the PTV and separated in the dose from all particles, only from neutrons and only from photons. Doses with a relative error above 80 % were ignored. (b) Neutron and photon dose divided by the absorbed dose, to observe their relative share. Doses with a relative error above 70 % were ignored.
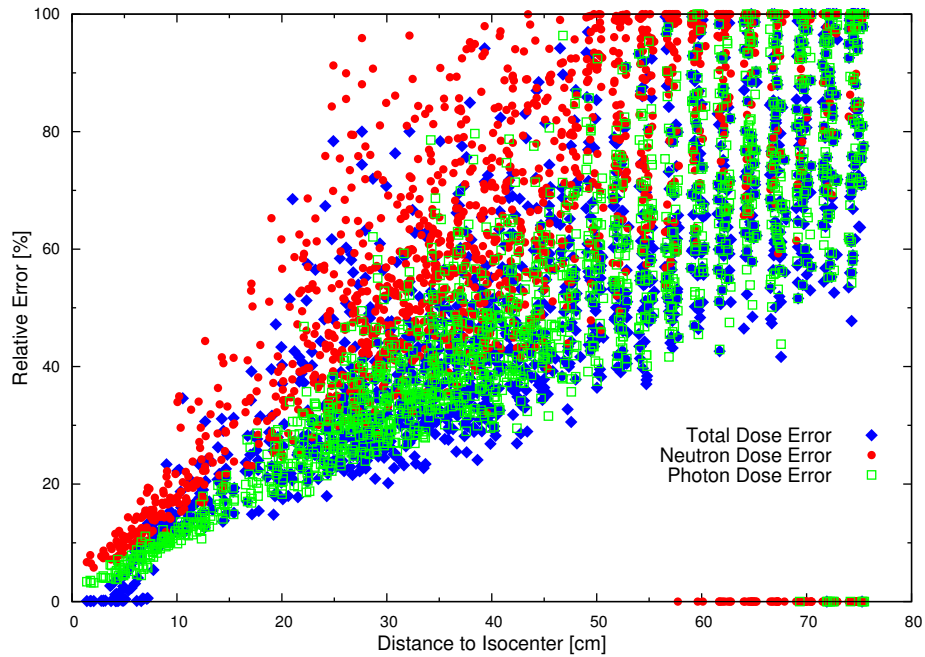
Figure 5.11.: Relative error of the dose deposited in every detector with the absolute distance to the isocenter of the PTV. A relative error of 0 % above 55 cm means that no dose was measured.

considerable contribution to the dose from protons takes place at $z = 4.5$ cm with proton energies from 0 to 70 MeV. These are scattered or secondary protons from the incoming beams. Photons have mainly energies between 0 and 10 MeV. This is also the case for neutrons, but there is also a contribution from higher energetic neutrons. According to the ICRP 60, neutrons with energies between 2 and 20 MeV have a radiation weighting factor ω_R of 10, while for neutrons above 20 MeV $\omega_R = 5$. Thus, due to their low amount of particles/cm^2 and their lower radiation weighting factor, neutrons above 20 or 30 MeV are not so important for a risk assessment.
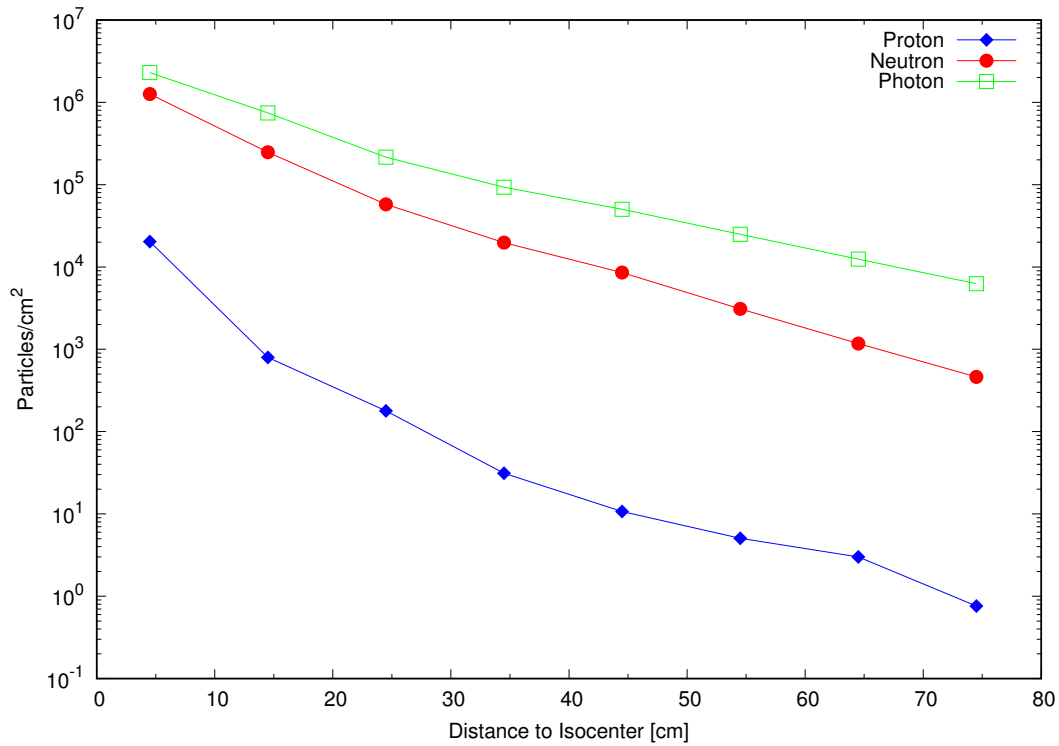
Figure 5.12.: Fluence of protons, neutrons and photons through xy-planes of the phantom. The distance to the isocenter is measured in the z-direction.
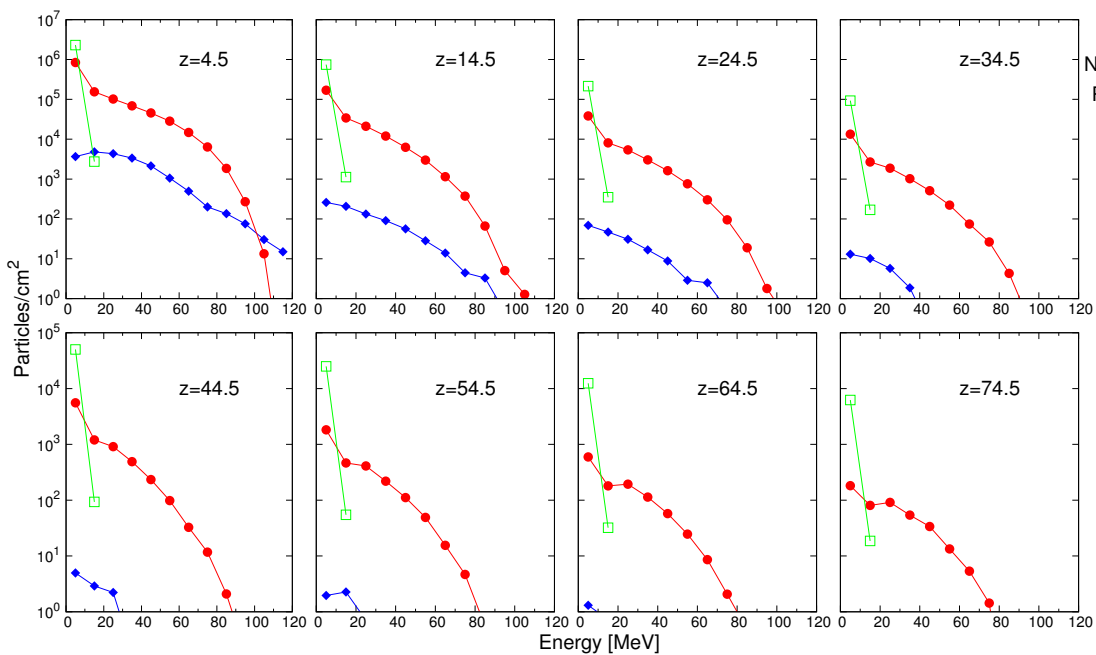
Figure 5.13.: Energy dependent fluence of protons, neutrons and photons in the xy-planes. The maximum energy of a beam was 124.7 MeV. Due to large uncertainties, values below one particle/cm^2 were ignored.

6. Summary

This study was, to the authors knowledge, the first attempt to transfer a treatment plan for proton therapy created by the treatment planning software RayStation 5 into an input file for the Monte-Carlo simulation code PHITS. The treatment plan was created for a RANDO® phantom with an imaginary brain tumor and exported in the DICOM format. The proton beam adopts the conditions met at the MedAustron accelerator in terms of beam parameters (pencil beam scanning). Furthermore a treatment plan for a simple watertank was created to validate the transfer procedure from RayStation to PHITS.

For the simulation in PHITS, the NUNDO (numerical RANDO®) phantom was used. The coordinate systems in RayStation and that in PHITS for the NUNDO had different origins. So it was necessary to find the isocenter of the beams in PHITS manually, which was a little bit tricky. This could have been avoided by using DICOM2PHITS, but DICOM2PHITS was not used due to several reasons mentioned in *Section 4.3*. The beam parameters (energy, position, spot size, etc.) were read out from the DICOM output by a Matlab program, corrected to match the isocenter position and written in dumpfiles for PHITS. Once this procedure is known, it is not hard to apply for future simulations. Using DICOM2PHITS could provide a further simplification.

It was shown that PHITS is able to reproduce the average dose from RayStation in the target very accurate within 1 %. Using ATIMA for energy straggling and multiple Coulomb scattering in PHITS brought the best results, but also Landau and Vavilov distributions and Lynch's formula based on the Moliere theory showed satisfying results (difference of 5 % for the average dose of the watertank target compared to RayStation). On the other side, detailed investigation of the dose distribution in- and outside the target and of line doses through the target exhibited fluctuations of the dose in PHITS, which were not present in RayStation.

The absorbed dose in organs and detectors decreases exponentially with distance. Ten cm away from the center of the target, the dose is in the mGy area and falls off to

around 1μ Gy at 80 cm distance. Above 10 cm distance to the target the dose is mainly produced by neutrons and photons and the share of the dose caused by neutrons decreases and that from photons increases with distance. At around 40 - 50 cm away from the target their shares are equal. A problem of the dose simulation in far distant detectors is their high uncertainty, which can only be reduced by increasing the number of particles and thus, the simulation time.

Finally can be said that the transfer of a treatment plan from RayStation to PHITS was largely successful and the results can be benchmarked with future experiments at the MedAustron. For a better agreement in the dose distribution in- and outside the target, it would be advisable to try different settings in PHITS (eg. different energy and angular straggling models) or to use another Monte-Carlo code.

Bibliography

[1] Particle Therapy Co-Operative Group. 2016. URL: https://www.ptcog.ch/index.php/patient-statistics.

[2] Emmanouil Fokas et al. "Ion beam radiobiology and cancer: Time to update ourselves". In: *Biochimica et Biophysica Acta (BBA) - Reviews on Cancer* 1796.2 (2009), pp. 216–229. ISSN: 0304-419X. DOI: http://dx.doi.org/10.1016/j.bbcan.2009.07.005. URL: http://www.sciencedirect.com/science/article/pii/S0304419X09000523.

[3] MedAustron. URL: https://www.medaustron.at/en.

[4] Tatsuhiko Sato et al. "Particle and Heavy Ion Transport code System, PHITS, version 2.52". In: *Journal of Nuclear Science and Technology* 50.9 (2013), pp. 913–923.

[5] S. Agostinelli et al. "Geant4—a simulation toolkit". In: *Nuclear Instruments and Methods in Physics Research Section A: Accelerators, Spectrometers, Detectors and Associated Equipment* 506.3 (2003), pp. 250–303. ISSN: 0168-9002. DOI: http://dx.doi.org/10.1016/S0168-9002(03)01368-8. URL: http://www.sciencedirect.com/science/article/pii/S0168900203013688.

[6] A. Ferrari et al. "FLUKA: a multi-particle transport code". In: *CERN 2005-10 (2005), INFN/TC 05/11, SLAC-R-773*.

[7] Daniel Matthiä, Thomas Berger, and Günther Reitz. "Organ shielding and doses in Low-Earth orbit calculated for spherical and anthropomorphic phantoms". In: *Advances in Space Research* 52.3 (2013), pp. 528–535. ISSN: 0273-1177. DOI: http://dx.doi.org/10.1016/j.asr.2013.03.025. URL: http://www.sciencedirect.com/science/article/pii/S0273117713001786.

[8] Robert R. Wilson. "Radiological Use of Fast Protons". In: *Radiology* 47.5 (1946), pp. 487–491. DOI: 10.1148/47.5.487. URL: http://dx.doi.org/10.1148/47.5.487.

[9]   Harald Paganetti. *Proton Therapy Physics -*. 1. Aufl. Boca Raton, Fla: CRC Press, 2016. ISBN: 978-1-439-83645-3.

[10]   L. Landau. "On the energy loss of fast particles by ionization". In: *J. Phys.(USSR)* 8 (1944), pp. 201–205.

[11]   P. V. Vavilov. "Ionization losses of high-energy heavy particles". In: *Sov. Phys. JETP* 5 (1957). [Zh. Eksp. Teor. Fiz.32,920(1957)], pp. 749–751.

[12]   G. Molière. "Theorie der Streuung schneller geladener Teilchen I. Einzelstreuung am abgeschirmten Coulomb-Feld". In: *Zeitschrift Naturforschung Teil A* 2 (Mar. 1947), pp. 133–145. DOI: 10.1515/zna-1947-0302.

[13]   G. Molière. "Theorie der Streuung schneller geladener Teilchen II. Mehrfach- und Vielfachstreuung". In: *Zeitschrift Naturforschung Teil A* 3 (Feb. 1948), pp. 78–97. DOI: 10.1515/zna-1948-0203.

[14]   URL: http://www.shi.co.jp/quantum/eng/product/proton/img/SOBP.png.

[15]   Chiara La Tessa et al. "Out-of-field dose studies with an anthropomorphic phantom: Comparison of X-rays and particle therapy treatments". In: *Radiotherapy and Oncology* 105 (2012), pp. 133–138. DOI: 10.1016/j.radonc.2012.04.004.

[16]   *RayStation 5*. URL: http://www.raysearchlabs.com/raystation5/.

[17]   Lembit Sihver. *private communication*.

[18]   A. Boudard et al. "New potentialities of the Liège intranuclear cascade model for reactions induced by nucleons and light charged particles". In: *Phys. Rev. C* 87 (1 Jan. 2013), p. 014606. DOI: 10.1103/PhysRevC.87.014606. URL: http://link.aps.org/doi/10.1103/PhysRevC.87.014606.

[19]   Shiori Furihata et al. "The GEM code: A simulation program for the evaporation and the fission process of an excited nucleus". In: *JAERI-Data/Code–2001-015* ().

[20]   Gerald R. Lynch and Orin I. Dahl. "Approximations to multiple Coulomb scattering". In: *Nucl. Instrum. Meth.* B58 (1991), pp. 6–10. DOI: 10.1016/0168-583X(91)95671-Y.

[21]   URL: https://web-docs.gsi.de/~weick/atima/.

[22]   Kei Iida, Akihisa Kohama, and Kazuhiro Oyamatsu. "Formula for proton-nucleus reaction cross section at intermediate energies and its application". In: *J. Phys. Soc. Jap.* 76 (2007), pp. 044201–044300. DOI: 10.1143/JPSJ.76.044201. arXiv: nucl-th/0601039 [nucl-th].

[23] L. Sihver et al. "Current status of the "Hybrid Kurotama model" for total reaction cross sections". In: *Nuclear Instruments and Methods in Physics Research Section B: Beam Interactions with Materials and Atoms* 334 (2014), pp. 34–39. ISSN: 0168-583X. DOI: `http://dx.doi.org/10.1016/j.nimb.2014.04.021`. URL: `http://www.sciencedirect.com/science/article/pii/S0168583X14005230`.

[24] M. Puchalska et al. "Simulations of {MATROSHKA} experiment outside the {ISS} using {PHITS}". In: *Advances in Space Research* 50.4 (2012), pp. 489–495. ISSN: 0273-1177. DOI: `http://dx.doi.org/10.1016/j.asr.2012.04.027`. URL: `http://www.sciencedirect.com/science/article/pii/S027311771200289X`.

[25] M. Puchalska et al. "NUNDO: a numerical model of a human torso phantom and its application to effective dose equivalent calculations for astronauts at the ISS". In: *Radiation and Environmental Biophysics* 53.4 (2014), pp. 719–727. DOI: `http://doi.org/10.1007/s00411-014-0560-7`.

[26] J. Valentin. "Basic anatomical and physiological data for use in radiological protection: reference values: ICRP Publication 89: Approved by the Commission in September 2001". In: *Annals of the ICRP* 32.3-4 (2002), pp. 1–277. DOI: `10.1016/S0146-6453(03)00002-2`. eprint: `http://ani.sagepub.com/content/32/3-4/1.full.pdf+html`. URL: `http://ani.sagepub.com/content/32/3-4/1.abstract`.

[27] Guenther Reitz et al. "Astronaut's organ doses inferred from measurements in a human phantom outside the international space station". In: *Radiation Research* 171.2 (Feb. 2009), pp. 225–235. ISSN: 0033-7587. DOI: `10.1667/RR1559.1`.

[28] L. Sihver et al. "Simulations of the MATROSHKA experiment at the international space station using PHITS". In: *Radiation and Environmental Biophysics* 49.3 (2010), pp. 351–357. ISSN: 1432-2099. DOI: `10.1007/s00411-010-0288-y`. URL: `http://dx.doi.org/10.1007/s00411-010-0288-y`.

Appendices

A. PHITS Input File

Listing A.1: Source section of the PHITS input file for one energy layer

```
<source> = 110              # number of spots in this energy layer
    s-type =  17            # external source with PHITS dump file
    file =  dumpfile0.dat  # file name of dump file
    dump =   -6             # number of dumped data <0: ascii, >0: binary
            1 2 3 4 9 8
    dir  = 0
    phi  = 180
    dom = 0.37033
```

B. Shielding Program

Listing B.1: Source code of the shielding program

```cpp
#include <iostream>
#include <fstream>
#include <string>
#include <cstdlib>
#include <cmath>
#include <ctime>
#include <vector>
using namespace std;


const double pi=atan(1)*4;

// random sphere
void sphere(double &x, double &y, double &z)
{
    double phi, theta;
    phi=((double)rand()/(RAND_MAX))*2*pi;
    theta=((double)rand()/(RAND_MAX))*2*pi;
    x=0.1*cos(theta)*sin(phi);
    y=0.1*sin(theta)*sin(phi);
    z=0.1*cos(phi);
}

double distance(double x1, double y1, double z1, double x2, double y2, double z2)
{
    return sqrt(pow(abs(x1)-abs(x2),2)+pow(abs(y1)-abs(y2),2)+pow(abs(z1)-abs(z2),2));
}

double round(double number, double i)
{
    return (int)(number*i+0.5)/i;
}

int main()
{
    const int px=357, py=269, air=99, remainder=801, ovaries=802, skin=803, lung=806, breast=807,
            stomach=808, thyroid=810, oesophagus=813, colon=814, bones=816, brain=818, liver=820,
            glands=823, redbone=826, bladder=831, testes=835;
    int i=0, j=0, k=0, n=0, m=0, number, x=0, y=0, z=0, position;
    double averagedistance=0, x_sphere, y_sphere, z_sphere, x_distance, y_distance, z_distance,
            x_round, y_round, z_round, x_position, y_position, z_position;
    vector<double> density, x_organ, y_organ, z_organ, x_zero, y_zero, z_zero, x_remainder,
```

```
                   y_remainder, z_remainder, x_ovaries, y_ovaries, z_ovaries, x_skin, y_skin,
                   z_skin, x_lung, y_lung, z_lung, x_breast, y_breast, z_breast, x_stomach,
                   y_stomach, z_stomach, x_thyroid, y_thyroid, z_thyroid, x_oesophagus,
                   y_oesophagus, z_oesophagus, x_colon, y_colon, z_colon, x_bones, y_bones,
                   z_bones, x_brain, y_brain, z_brain, x_liver, y_liver, z_liver, x_glands,
                   y_glands, z_glands, x_redbone, y_redbone, z_redbone, x_bladder, y_bladder,
                   z_bladder, x_testes, y_testes, z_testes;
srand(time(NULL));

ifstream filein ("voxel.inp");
if(!filein)
{
    cout << "File not found." << endl;
    system("PAUSE");
    return(1);
}
i=0;
// reading of the voxel file and assign the positions
while (filein >> number)
{
    if(x==px+1)
    {
        x=0;
        y++;
    }
    if(y==py+1)
    {
        y=0;
        z++;
    }

    if(number==air) density.push_back(0);
    else if(number==lung) density.push_back(0.352);
    else if(number==bones) density.push_back(1.3);
    else density.push_back(0.997);

    if(number==remainder)
    {
        x_remainder.push_back(double(x)*0.1);
        y_remainder.push_back(double(y)*0.1);
        z_remainder.push_back(double(z)*0.5);
    }
    if(number==ovaries)
    {
        x_ovaries.push_back(double(x)*0.1);
        y_ovaries.push_back(double(y)*0.1);
        z_ovaries.push_back(double(z)*0.5);
    }
    if(number==skin)
    {
        x_skin.push_back(double(x)*0.1);
        y_skin.push_back(double(y)*0.1);
        z_skin.push_back(double(z)*0.5);
```

```
    }
    if (number==lung)
    {
        x_lung.push_back(double(x)*0.1);
        y_lung.push_back(double(y)*0.1);
        z_lung.push_back(double(z)*0.5);
    }
    if (number==breast)
    {
        x_breast.push_back(double(x)*0.1);
        y_breast.push_back(double(y)*0.1);
        z_breast.push_back(double(z)*0.5);
    }
    if (number==stomach)
    {
        x_stomach.push_back(double(x)*0.1);
        y_stomach.push_back(double(y)*0.1);
        z_stomach.push_back(double(z)*0.5);
    }
    if (number==thyroid)
    {
        x_thyroid.push_back(double(x)*0.1);
        y_thyroid.push_back(double(y)*0.1);
        z_thyroid.push_back(double(z)*0.5);
    }
    if (number==oesophagus)
    {
        x_oesophagus.push_back(double(x)*0.1);
        y_oesophagus.push_back(double(y)*0.1);
        z_oesophagus.push_back(double(z)*0.5);
    }
    if (number==colon)
    {
        x_colon.push_back(double(x)*0.1);
        y_colon.push_back(double(y)*0.1);
        z_colon.push_back(double(z)*0.5);
    }
    if (number==bones)
    {
        x_bones.push_back(double(x)*0.1);
        y_bones.push_back(double(y)*0.1);
        z_bones.push_back(double(z)*0.5);
    }
    if (number==brain)
    {
        x_brain.push_back(double(x)*0.1);
        y_brain.push_back(double(y)*0.1);
        z_brain.push_back(double(z)*0.5);
    }
    if (number==liver)
    {
        x_liver.push_back(double(x)*0.1);
        y_liver.push_back(double(y)*0.1);
```

```
            z_liver.push_back(double(z)*0.5);
        }
        if(number==glands)
        {
            x_glands.push_back(double(x)*0.1);
            y_glands.push_back(double(y)*0.1);
            z_glands.push_back(double(z)*0.5);
        }
        if(number==redbone)
        {
            x_redbone.push_back(double(x)*0.1);
            y_redbone.push_back(double(y)*0.1);
            z_redbone.push_back(double(z)*0.5);
        }
        if(number==bladder)
        {
            x_bladder.push_back(double(x)*0.1);
            y_bladder.push_back(double(y)*0.1);
            z_bladder.push_back(double(z)*0.5);
        }
        if(number==testes)
        {
            x_testes.push_back(double(x)*0.1);
            y_testes.push_back(double(y)*0.1);
            z_testes.push_back(double(z)*0.5);
        }
        x++;
    }
    filein.close();

    x_zero.push_back(0);
    y_zero.push_back(0);
    z_zero.push_back(0);

    ofstream fileout ("distance.dat");
    fileout << "#organ    shielding    points" << endl;

    for(k=801; k<836; k++)
    {
        n=0;
        averagedistance=0;
        switch(k)
        {
            case 801: x_organ=x_remainder;
                      y_organ=y_remainder;
                      z_organ=z_remainder;
                      break;
            case 802: x_organ=x_ovaries;
                      y_organ=y_ovaries;
                      z_organ=z_ovaries;
                      break;
            case 803: x_organ=x_skin;
                      y_organ=y_skin;
```

```
          z_organ=z_skin;
          break;
case 804: x_organ=x_zero;
          y_organ=y_zero;
          z_organ=z_zero;
          break;
case 806: x_organ=x_lung;
          y_organ=y_lung;
          z_organ=z_lung;
          break;
case 807: x_organ=x_breast;
          y_organ=y_breast;
          z_organ=z_breast;
          break;
case 808: x_organ=x_stomach;
          y_organ=y_stomach;
          z_organ=z_stomach;
          break;
case 809: x_organ=x_zero;
          y_organ=y_zero;
          z_organ=z_zero;
          break;
case 810: x_organ=x_thyroid;
          y_organ=y_thyroid;
          z_organ=z_thyroid;
          break;
case 811: x_organ=x_zero;
          y_organ=y_zero;
          z_organ=z_zero;
          break;
case 813: x_organ=x_oesophagus;
          y_organ=y_oesophagus;
          z_organ=z_oesophagus;
          break;
case 814: x_organ=x_colon;
          y_organ=y_colon;
          z_organ=z_colon;
          break;
case 815: x_organ=x_zero;
          y_organ=y_zero;
          z_organ=z_zero;
          break;
case 816: x_organ=x_bones;
          y_organ=y_bones;
          z_organ=z_bones;
          break;
case 817: x_organ=x_zero;
          y_organ=y_zero;
          z_organ=z_zero;
          break;
case 818: x_organ=x_brain;
          y_organ=y_brain;
          z_organ=z_brain;
```

```
                        break ;
        case  819:  x_organ=x_zero ;
                    y_organ=y_zero ;
                    z_organ=z_zero ;
                        break ;
        case  820:  x_organ=x_liver ;
                    y_organ=y_liver ;
                    z_organ=z_liver ;
                        break ;
        case  821:  x_organ=x_zero ;
                    y_organ=y_zero ;
                    z_organ=z_zero ;
                        break ;
        case  823:  x_organ=x_glands ;
                    y_organ=y_glands ;
                    z_organ=z_glands ;
                        break ;
        case  824:  x_organ=x_zero ;
                    y_organ=y_zero ;
                    z_organ=z_zero ;
                        break ;
        case  826:  x_organ=x_redbone ;
                    y_organ=y_redbone ;
                    z_organ=z_redbone ;
                        break ;
        case  827:  x_organ=x_zero ;
                    y_organ=y_zero ;
                    z_organ=z_zero ;
                        break ;
        case  831:  x_organ=x_bladder ;
                    y_organ=y_bladder ;
                    z_organ=z_bladder ;
                        break ;
        case  832:  x_organ=x_zero ;
                    y_organ=y_zero ;
                    z_organ=z_zero ;
                        break ;
        case  835:  x_organ=x_testes ;
                    y_organ=y_testes ;
                    z_organ=z_testes ;
                        break ;
    }

    for (m=0; m<x_organ . size ( ) ;  m++)
    {
        for ( j =0;  j <50;  j ++)
        {
            position=x_organ [m] *10+ y_organ [m] *3580+ z_organ [m] *193320;
            x_position=x_organ [m] ;
            y_position=y_organ [m] ;
            z_position=z_organ [m] ;

            i =0;
```

```
            sphere(x_sphere, y_sphere, z_sphere);

            while(density[position]!=0)
            {
                i++;

                x_distance=x_organ[m]+i*x_sphere;
                y_distance=y_organ[m]+i*y_sphere;
                z_distance=z_organ[m]+i*z_sphere;

                if(x_distance<0 || y_distance <0 || z_distance<0 || x_distance >35.7 ||
                    y_distance >26.9 || z_distance >84.5) break;

                x_round=round(x_distance, 10.0);
                y_round=round(y_distance, 10.0);
                z_round=round(z_distance, 2.0);

                position=x_round*10+y_round*3580+z_round*193320;

                averagedistance=averagedistance+distance(x_position, y_position, z_position,
                            x_distance, y_distance, z_distance)*density[position];

                x_position=x_distance;
                y_position=y_distance;
                z_position=z_distance;
            }
            n++;
        }
    }
    averagedistance=averagedistance/n;
    if(x_organ.size()>10) fileout << k << "   " << averagedistance << "   " << x_organ.size() << endl;
    }
    fileout.close();
    return(0);
}
```